Cover Page

Evolution and architecture of an exhumed ocean-facing coarse-grained submarine canyon fill, Baja California, Mexico

Authors: **Max J. Bouwmeester**[1], Ian A. Kane[1], David M. Hodgson[2], Stephen S. Flint[1], William J. Taylor[2], Euan L. Soutter[1], Adam D. McArthur[2], Miquel Poyatos-Moré[3], Joshua Marsh[1], Ed Keavney[2], Rufus L. Brunt[1], Victoria Valdez-Buso[4],

Affiliations: [1] University of Manchester; [2] University of Leeds; [3] Universitat Autònoma de Barcelona; [4] Universidade Federal do Paraná

Contact: max.bouwmeester@manchester.ac.uk | @max_bouwmeester

This paper is a non-peer reviewed preprint submitted to EarthArXiv.

This preprint was submitted to the journal Sedimentology for peer review.

Evolution and architecture of an exhumed ocean-facing coarse-grained submarine canyon fill, Baja California, Mexico

Authors: **Max J. Bouwmeester[1]**, Ian A. Kane[1], David M. Hodgson[2], Stephen S. Flint[1], William J. Taylor[2], Euan L. Soutter[1], Adam D. McArthur[2], Miquel Poyatos-Moré[3], Joshua Marsh[1], Ed Keavney[2], Rufus L. Brunt[1], Victoria Valdez-Buso[4],

Affiliations: [1] University of Manchester; [2] University of Leeds; [3] Universitat Autònoma de Barcelona; [4] Universidade Federal do Paraná

Key words: Active margin; Cretaceous; Facies; Architecture; Strike-slip tectonics; Flow processes

Abstract

Present day submarine canyons are active conduits for large volumes of sediment, carbon, and pollutants from continents to oceans. However, the evolution of submarine canyons over geological timescales remains poorly understood due to their erosional nature and low preservation potential. The Late Cretaceous Punta Baja Formation represents a well-preserved submarine canyon-fill on a tectonically-active ocean-facing margin. Outcrops provide km-scale continuous strike and dip sections of the 120 m thick and 1.2 km wide feature. An inherited tectonic fabric influenced the location and orientation of canyon incision into fluvial bedrock. The stratigraphic evolution of the Punta Baja submarine canyon is reconstructed from incision to fill, and shows that it remained an active sediment conduit throughout the time period represented by the preserved fill. The depositional architecture of the north-south oriented erosionally confined canyon-fill is asymmetric, with sub-vertically stacked channel-fills to the west, and an overbank confined by the canyon margin in the east. Sedimentary process interactions led to depositional patterns that we consider distinct to submarine canyon fills. Dynamic topography created by mass wasting processes captured sediment and drove knickpoint development, an autogenic mechanism that modifies sediment delivery to the ocean floor. We interpret widespread upstream dipping surfaces in channel-fills as the stratigraphic expression of migrating supercritical-flow bedforms, playing an important role in sediment storage and transport in the canyon. The proximal location of canyons and unique confinement configuration impact transverse and lateral gravity flow filtering, causing depositional patterns in the intra-canyon overbank areas that are less well organised than in published examples of external levees and which were previously poorly characterised for submarine canyons. This study provides insight into how processes that are observed in modern canyons are selectively preserved through the lifetime of the canyon and construct or destroy stratigraphy on geological timescales.

1 Introduction

Submarine canyons funnel large volumes of sediment from continents to oceans via gravity flows (Daly, 1936; Kuenen, 1938; Shepard, 1972; Fildani, 2017; Fisher *et al.*, 2021). More than 9,500 submarine canyons mapped along the Earth's continental margins (Harris *et al.*, 2014) are now recognised to play an important role in ocean circulation patterns (Allen & Durrieu De Madron, 2009; Zhu *et al.*, 2010; Nazarian *et al.*, 2021), marine biodiversity (Schlacher *et al.*, 2007; Bianchelli *et al.*, 2010; Vetter *et al.*, 2010; Fernandez-Arcaya *et al.*, 2017), and carbon and pollutant export from shelves to deep water locations (Palanques *et al.*, 2008; Pham *et al.*, 2014; Puig *et al.*, 2014; Hage *et al.*, 2020; Taviani *et al.*, 2023). Despite their size and ubiquity, little is known about how sediment in submarine canyons is stored and transferred into the stratigraphic record on geological timescales. Direct monitoring studies over the last decade are challenging paradigms in submarine canyon sediment dynamics, showing that sediment transport in canyons is more frequent (Heijnen *et al.*, 2022b), powerful (Paull *et al.*, 2018), longer-lasting (Azpiroz-Zabala *et al.*, 2017), and dynamic (Clare *et al.,* 2023; Lo Iacono *et al.*, 2020; Aslam *et al.*, 2018) than previously thought (Normark & Piper, 1991). Subsurface studies reveal stacking patterns and internal architectures (e.g. Almgren & Hacker, 1984; Galloway *et al.*, 1991; Rasmussen, 1994; Hsieh *et al.*, 2020; Su *et al.*, 2020; Fisher *et al.*, 2021; Tian *et al.*, 2021; Li *et al.*, 2022; Wu *et al.*, 2022) but lack the finer-scale sedimentological detail that outcrop studies can provide. However, exhumed submarine canyon fills are rare, particularly from ocean-facing systems, and typically have limited downdip control (Von der Borch *et al.*, 1985; Advocate *et al.*, 1988; Millington & Clark, 1995; Seidler, 2000; May & Warme, 2007; Di Celma & Cantalamessa, 2012; Ito *et al.*, 2014; Dasgupta & Buatois, 2015; McArthur & McCaffrey, 2019; Janocko & Basilici, 2021).

Here, we document the exceptionally well-preserved fill of a submarine canyon that formed on an active tectonic margin of Baja California. Coarse-grained systems of the Cretaceous-Paleogene Rosario Formation have been heavily studied, focussing on the lower canyon to channel-levee environments (Morris & Busby-Spera, 1990; Kane *et al.*, 2009; Li *et al.*, 2018; Kneller *et al.*, 2020). Less studied exposures of the Late Cretaceous Punta Baja Formation provide continuous depositional strike and dip sections of the 120 m thick and 1.2 km wide feature, with 4.5 km of continuous dip exposure. Canyon inception and evolution has been linked to tectonics causing severe baselevel changes, constraining the canyon's lifespan to a maximum of 8 Myr (Kane *et al.*, 2022). Multi-scale depositional architecture and depositional environments are interpreted using mapping, sedimentary logging, high-resolution photogrammetry, and detailed facies descriptions. New facies models for submarine canyon deposits are presented, and compared to other deep-marine environments to discuss flow dynamics in submarine canyons. Using the continuous strike and dip sections, this study reconstructs the evolution of the submarine canyon from incision, through infill, to burial.

We show that the Punta Baja submarine canyon-fill is asymmetric in strike section, and how mass wasting processes impacted canyon architecture and evolution. We provide a rare continuous dip-section through canyon-axis deposits, and show that the Punta Baja submarine canyon remained a highly dynamic and erosion-bypass dominated conduit during its infill. Abundant upstream dipping surfaces are quantified and interpreted to represent the stratigraphic expression of supercritical upstream migrating knickpoints and dunes. Facies types and distributions are more complex compared to other deep-marine conduit environments, owing to the unique configuration of confinement, remobilisation of unstable margins, and proximity to the sediment source and sites of flow generation, in submarine canyons.

2 Geological Setting

Late Cretaceous-Paleogene sediments were deposited in the Pacific Ocean-facing fore-arc basin of the Peninsular Ranges (Beal, 1948; Gastil *et al.*, 1975; Busby *et al.*, 2006). The Peninsular Ranges formed in the Early Jurassic as the intra-oceanic Alisitos Arc (Gastil *et al.*, 1975; Busby *et al.*, 1998, 2006), accreting onto North America until 105 Ma (Busby *et al.*, 2006; Alsleben *et al.*, 2012) by the oblique subduction of the Farallon plate under North America (Hagstrum *et al.*, 1985). This collision translated the arc northwards (Hagstrum *et al.*, 1985) and transformed the region into a compressional continental arc (Busby *et al.*, 1998, 2006; Busby, 2004). Subduction under the arc system led to the development of the gabbro-rich western part of Peninsular Ranges batholith in the latest Jurassic to Early Cenozoic (*Fig. 1*) (Hagstrum *et al.*, 1985; Busby *et al.*, 1998; Kimbrough *et al.*, 2015). Pre-batholitic rocks contain detrital zircons sourced from the North American craton, implying that the Alisitos system was a fringing arc (Busby *et al.*, 2006; Kimbrough *et al.*, 2015), conflicting with some authors suggesting a more exotic origin (Johnson *et al.*, 1999; Dickinson & Lawton, 2001; Wetmore *et al.*, 2002, 2014; Alsleben *et al.*, 2012). Magmatism culminated in the Late Cretaceous (98-92 Ma) with the La Posta granodiorite plutonic suite (Kimbrough *et al.*, 2006), causing regional uplift and deformation (Kimbrough *et al.*, 2001), before the locus of magmatism shifted eastward into mainland Mexico due to younging of subducting oceanic crust, which decreased the subduction angle (Moxon & Graham, 1987; Lipman, 1992; Mcdowell *et al.*, 2001; Sedlock, 2003; Busby, 2004). In the Late Cretaceous, transpressional tectonics and magmatism caused regional tilting manifested by uplift in the Peninsular ranges and subsidence to the west (Fig. 2); this uplift provided sediment for deposition of the fluvial Bocana Roja Formation (Turonian), the deep-marine Punta Baja Formation (Coniacian), the shallow-marine to fluvial El Gallo Formation (Campanian), the deep-marine Rosario Formation (Maastrichtian-Danian), and the volcanic-sedimentary Sepultura Formation (Paleocene) (*Fig. 1*) in the west-facing fore-arc basin onlapping the Peninsular Ranges (Beal, 1948; Gastil *et al.*, 1975).

The Peninsular Ranges supplied the Late Cretaceous sedimentary systems with a range of volcanic, intrusive, metamorphic, and sedimentary (carbonate, volcaniclastic, and siliciclastic) lithologies, across a short and steep basin margin (Fig. 1,2). Rapid tectonically-forced base-level changes, faulting and basinward tilting controlled the juxtaposition of continental and marine sedimentary systems (Busby *et al.*, 1998; Kane *et al.*, 2022).

The conduit documented in this study is preserved as the Punta Baja Formation submarine canyon-fill, which was steeply incised into the fluvial Bocana Roja Formation bedrock, filled, planed off and onlapped by the shallow-marine El Gallo Formation (*Fig. 1*) in a timespan of less than 8 Myr (derived from Detrital Zircon dating, Kane *et al.*, 2022). This succession of depositional environments has been described previously (Kilmer, 1963; Schile, 1974; Boehlke & Abbott, 1986; Morris & Busby, 1996; Kane *et al.*, 2022) and is further contextualised below.

2.1 La Bocana Roja Formation (Turonian)

The Bocana Roja Formation is the oldest sedimentary unit in the study area (93.6±1.1 Ma Maximum Depositional Age (MDA) derived from Large-N Detrital Zircon dating (Fig. 3, Kane *et al.* (2022)). The contact with the underlying Alisitos arc is not exposed (Kilmer, 1963; Schile, 1974). The Bocana Roja Formation is a ~675 – 1260 m-thick succession of maroon and grey siltstones, sandstones, and conglomerates, interpreted as overbank and braided stream deposits in a rapidly subsiding basin, with transport to the SW (Morris & Busby, 1996). The mudstones are mottled and contain calcrete horizons, indicating palaeosol formation (Morris & Busby, 1996). The sandstones are thick-bedded medium- to coarse-grained feldspathic volcanic litharenites, commonly with large trough cross-beds (Schile, 1974) and form 10 m-thick single-storey channel-fills with several types of conglomerate (clast- and matrix-supported, cross-bedded to massive) (Morris & Busby, 1996). Abundant black chert clasts and subordinate green, brown, and purple fine-grained and porphyritic volcanoclastic clasts are common (Kilmer, 1963). The unit is more tectonically deformed than overlying formations, tilted up to 40° to the south on the western margin, and 1-18° towards the west on the eastern margin, forming a broad syncline which is heavily faulted, possibly influencing subsequent Punta Baja Formation canyon incision (Kane *et al.*, 2022).

2.2 Punta Baja Formation (Coniacian – Santonian)

The Punta Baja Formation basal surface truncates the Bocana Roja Formation steeply by at least 140 m, forming a SSW-NNE trending depression 1.2 km wide (Boehlke & Abbott, 1986; Kane *et al.*, 2022). The infill (87.1±1.5 Ma MDA, Fig. 3, Kane *et al.* (2022)) is dominated by pebble-cobble conglomerate deposits on the western margin, with large clasts of the underlying Bocana Roja Formation bedrock overlying the basal surface (Kane *et al.*, 2022). To the east, these conglomerates grade through wedge-shaped sandstone bodies into thin-bedded turbidites that onlap the erosive surface in the east (Kane *et al.*, 2022). Macro- and micropalaeontology suggest depositional environments beyond the shelf-edge (Kane *et al.*, 2022) with water depths ranging from 600 – 2000 m (Boehlke & Abbott, 1986). These deposits have been interpreted as channel cut-and-fill, overbank, and crevasse-splay deposits of a submarine canyon that transported sediment towards the SSW (Boehlke & Abbott, 1986; Morris & Busby, 1996; Kane *et al.*, 2022). Conglomerate clasts are well-rounded and consist predominantly of metamorphosed, silicified intermediate volcanics, and related volcaniclastics and siliciclastic deposits most likely derived from the Alisitos Formation (>25 km distance), with minor quartzite clasts from a terrane further to the east (>100 km distance) (Boehlke & Abbott, 1986). A change in source area for the Punta Baja Formation compared to the Bocana Roja Formation is suggested by slightly different detrital zircon signatures (Kane *et al.*, 2022). The strata are uniformly tilted 2-5° to the E-SE, with local dips of up to 30° due to sedimentary onlap of the canyon wall (Boehlke & Abbott, 1986; Kane *et al.*, 2022). The Punta Baja Formation is less tectonically deformed than the Bocana Roja Formation, but displays several syn-depositional faults trending NNE-SSW (Kane *et al.*, 2022).

2.3 El Gallo Formation (Santonian – Maastrichtian)

The El Gallo Formation overlies both the Bocana Roja and Punta Baja formations with an angular unconformity, interpreted as a wave-ravinement surface in the Punta Baja area (Kane *et al.*, 2022). The basal surface is locally overlain by a transgressive cobble lag with bored clasts (Kane *et al.*, 2022). Farther east (20-50 km), the El Gallo Formation directly onlaps the Alisitos arc (Kilmer, 1963). The El Gallo Formation (86.8±1.8 Ma MDA, Fig. 3, Kane *et al.* (2022)) has a maximum thickness of 1.3 km and is divided into the La Escarpa Member (alluvial fan to braided stream deposits), overlain by the tuffaceous El Disecado Member (fluvial to tidal deposits) that grades eastwards into the poorly-sorted conglomeratic El Castillo Member (Kilmer, 1963; Schile, 1974; Morris & Busby, 1996; Fastovsky *et al.*, 2020). Conglomerates in this unit contain mainly rhyolitic, andesitic, granitic, and dolerite clasts (Schile, 1974).

3 Methods

The Punta Baja Formation canyon fill is exposed around the hamlet of Punta Baja (29°57'20.8"N 115°48'25.0"W), and in coastal cliffs around the Punta Baja peninsula. Desert climate conditions facilitate a general lack of vegetation and therefore excellent continuous exposures. Modern marine terraces are present across the field area, which can be distinguished by their (sub-) horizontal bedding orientation and abundant recent shell material. Recent semi- to un-consolidated sand dunes overlie stratigraphy in places. The northernmost coastal part of the field area could not always be accessed or photographed with Uncrewed Aerial Vehicles (UAVs) due to considerations with the local inhabitants.

Formation- and facies-mapping data in the 2.5x5 km study area using handheld GPS, the ArcGIS Field Maps application, the FieldMOVE Clino application, and geological compass was collated and processed in ArcGIS software. We recorded sedimentary and stratigraphic characteristics by measuring sections at 1:12.5 to 1:50 scale, systematically recording bed thickness and boundary surface type, median grain size and texture, clast orientation and median-largest clast size, sedimentary and diagenetic structures, bioturbation type and degree, palaeocurrent indicators from clast imbrication, ripple foresets, flutes, and grooves. We recorded a total of 450 m stratigraphic thickness across 41 logs. Correlations of surfaces or intervals were achieved by walking out these features where possible, aided by UAV imagery where necessary. We flew DJI Phantom 2 Pro and DJI Mavic Mini 2 UAVs to collect aerial photographs, with which 2.3 km^2 of detailed 3D outcrop models were constructed using photogrammetry software Agisoft Metashape. All models are available on V3Geo (See Supplementary materials).

Paleocurrent reconstructions (Supplementary materials) are presented in equal-area rose diagrams (Nemec, 1988) and subdivided per indicator type (Python code in supplementary materials). Stratigraphic cross-sections are based on elevation profiles derived from our combined UAV 3D outcrop model Digital Elevation Model (DEM), mapping, and measured sections.

We measured the orientation of fault planes using a geological compass and recorded their location, trace, and apparent offset using the FieldMOVE

Clino application and the ArcGIS Field Maps application. Where possible, we derived fault kinematics directly from offset stratigraphy, drag folds, shear along fault planes, and slickensides. Where fault offsets were unclear or complex, we recorded the orientation of conjugate fault sets to analyse for Riedel-shear sense-of-slip indicators. Because the surface expression of most major fault zones in the field area could be explained by pure strike-slip, pure vertical motion, or a combination of both, we indicate both components on the map (Fig. 4) without detailing the relative contributions of strike-slip and vertical motion. We analysed the orientation of fault planes per formation (Bocana Roja or Punta Baja), type (normal/reverse or transform), and location (north-west or south-east). The data (Supplementary materials) were plotted using Stereonet11 software (Allmendinger *et al.*, 2013; Cardozo & Allmendinger, 2013) on equal-area stereonets as poles to fault planes, after which clustering was determined using Kamb's contouring (Kamb, 1959). We filtered the data according to these variables to derive the signature of each in the complete dataset (Supplementary materials). We fitted planes to clusters in the dataset to derive mean fault orientations. The dominant fault characteristics are then carried over to the bigger groupings of data (Fig. 4).

Beds were assigned to facies and facies associations, and their recorded characteristics grouped and analysed accordingly. Logged facies, grain-size and bed thickness characteristics were plotted as Kernel Density Estimates (KDE) of number of beds to represent the entire dataset, with the mean, 5^{th} percentile, and 95^{th} percentile extracted as summary statistics. Representative facies distributions within each facies association were calculated by stratigraphic thickness. The ratio between coarse (very fine sand and coarser) and fine-grained (silt and finer) sediment was calculated per measured section and per environment, scaled by stratigraphic thickness. The coarse:fine values of heterolithic facies were estimated in the field based on sand-to-mud thickness ratio.

Since averaged coarse:fine ratios carry no information on the distribution of lithologies within any given interval, we provide another parameter representing heterogeneity. We define heterogeneity here in a purely vertical stratigraphic sense, by the number of changes between coarse and fine lithologies per metre of measured stratigraphy (changes per metre or c/m). Together with the averaged coarse:fine ratio values, this characterises facies and environments in a useful way for subsurface applications.

The orientation of surfaces was approximated by interpreting lines (via points) on our high-resolution 3D outcrop models in LIME software (Buckley *et al.*, 2019) (Supplementary materials). To each surface point cloud, a plane was fitted using Singular Value Decomposition (SVD), which yielded a dip direction, dip angle, spatial coordinates of the centre point, and point cloud maximum diameter (Python code and data in supplementary materials). Out of all interpreted surfaces (n=631), obvious non-planar surfaces and steep erosional features marked during interpretation were excluded to yield all sedimentary surfaces (n=539). These were then plotted on a map and their dip direction was compared to the mean paleocurrent direction in the canyon indicated by conglomerate clast imbrication. Post-sedimentary tectonic tilting in the study area was minimal, but generally to the E-SE. This might result in an overrepresentation of downstream and eastwards dipping surfaces, but since the dip angle of the surfaces (>5°) is generally steeper than the regional tectonic tilt (2 – 5°), this is not considered problematic.

We collected two samples for large-N Detrital Zircon dating in addition to the previously published dataset of Kane et al. (2022). Detrital Zircons for both studies were extracted and processed at the University of Calgary. U/Pb ratios and dates of three hundred grains from each sample (n=9) were obtained using Laser Ablation – Inductively Coupled – Plasma Mass Spectrometry (LA –ICP–MS) following the methodology of Matthews & Guest (2016). Sandstone maximum depositional ages (MDAs) were (re-)calculated using the YGC 2σ methodology (Dickinson & Gehrels, 2009) and analysed using a modified version of detritalPy (Sharman *et al.*, 2018) (Fig. 3). Where possible, the youngest detrital zircon grains were reablated to test the isotopic homogeneity of the grain(s) used in the calculation of the MDA and to reduce uncertainty (Spencer et al. 2016).

Micropaleontological (N = 2) and palynological (N = 2) samples were collected to compare with those documented in Kane *et al.* (2022) and processed in a standard fashion (Wood *et al.*, 1996). Residues were analysed for their organic matter content and identification of key dinoflagellate cyst species. Species were compared with published regional age ranges to determine an acme age range and depositional environment.

4 Results

4.1 Structural control on canyon evolution

General structural fabric

Structural deformation in the study area is dominated by normal faults, dipping 60°±10° to the SW or NNE. Strike-slip faults occur generally as near-vertically dipping (80 – 90°) NNE-SSW trending fault zones, and more rarely trending in a perpendicular WNW-ESE direction (Fig. 4). Reverse faults are rare (n=6), generally dipping 30 – 40° to the NE. The perpendicular orientation of strike-slip and normal-reverse faults in the study area is consistent with a locally extensional transform stress regime, often seen in releasing bends or step-over zones in transform systems (Reading, 1980; Rodgers, 1980; Christie-Blick & Biddle, 1985; Wu *et al.*, 2009; Huang & Liu, 2017).

The sense of movement along brittle strike-slip faults is difficult to establish in the field, without clear indictors such as slickensides or offset lithological boundaries. We analysed conjugate fault sets and compared their orientation to kinematic models of Riedel shear, but the measured orientations were often incompatible with existing models of Riedel shear. This might be due to the rheology of coarse sandstones and conglomerates, or the oblique-slip stress regime. Compatible orientations tentatively indicate a dextral strike-slip sense for NE-SW trending faults, which agrees with the regional stress regime related to the oblique subduction and northward translation of the arc terrain relative to North America.

Bedrock deformation

The Bocana Roja Formation bedrock is dominantly normal faulted, with antithetic 60°-dipping fault planes. The dominant failure direction in the NW of the study area is towards the SW, while on the opposite side of the canyon fill in the SE, the failure direction is dominantly to the NE (Fig. 4). This antithetic spatial distribution of extensional faults is interpreted to represent opposing extremities of a releasing bend.

The SW-NE trending strike-slip lineament and the extensional normal faults in the Bocana Roja Formation bedrock forming in a releasing bend of a transform zone likely steered and accommodated the Punta Baja canyon as a conduit. This explains the SSW-directed sediment transport within the canyon (Fig. 4), which diverges from the regional westwards trend of sedimentary systems that is perpendicular to the paleo-slope (Fig. 1,2) (Kane *et al.*, 2022).

Canyon fill deformation

The strike-slip faults in the Punta Baja canyon-fill trend SSW-NNE, at a slight angle with the SW-NE trending faults in the Bocana Roja Formation bedrock. This difference might be due to rotation of the Bocana Roja Formation due to the ongoing transform faulting during Punta Baja Formation deposition. This rotation could be accommodated in rotational blocks documented in transform shear zones and releasing/constraining bends (Christie-Blick & Biddle, 1985). The NW-SE trending transform fault signature in the study area likely represents the shear zones that bound the rotational blocks, consistent with the sinistral sense of shear observed in some of these fault zones.

The reverse faulting in the northern segment of the Punta Baja canyon-fill is directed SW-wards and might indicate either tectonic inversion in the northern section of the releasing bend, or syn-depositional down-slope failure and the compressional ‘toe’ of mass wasting of the canyon deposits. Normal faulting in the SE segment of the Punta Baja canyon-fill might represent sedimentary failure of canyon deposits into the conduit due to sedimentary oversteepening or tectonic activity. We recognised no definitive indicators for the syn- or post-depositional nature of these faults in the field.

4.2 Facies and depositional environments

4.2.1 AXIS – submarine braid plain

Description: This facies association is up to 30 m thick, overlies a basal erosion surface, and is characterised by thin- to thick-bedded highly amalgamated conglomerates and sandstones, with minor heterolithic intervals. This facies association has the lowest mud-content by stratigraphic thickness and is the most homogeneous. The succession is dominated by thick-bedded organised (Co) and disorganised (Cu) conglomerates, commonly with erosive bases and/or within successions confined by steep erosion surfaces (Fig. 6d,f). Cross-bedded conglomerate or conglomerate-sandstone (CSx) is found in tabular packages up to 2 m thick (Fig. 6c), or as wedges that commonly overlie mudclast breccia (Dm) that form concave-up lenses (Fig. 6g). Sub-horizontal interstratified conglomerates and sandstones (CSh) provide the most laterally continuous beds of the facies association, with minor variations in bed thickness along their length (Fig. 6c). These facies may be truncated by metre-scale erosion surfaces overlain by massive sandstone (ST) with minor gravel lags (Fig. 6e). Thinner-bedded sandstone (ST) and heterolithics (H) are seen overlying and onlapping conglomerates in finning- and thinning-upwards successions up to 3 m thick.

Interpretation: We interpret this facies association as submarine braid plain deposits (Klaucke & Hesse, 1996; Hesse *et al.*, 2001). Conglomerate deposition on the submarine braid plain was governed by non-cohesive debris flows (Walker, 1975; Lowe, 1982; Postma *et al.*, 1988; Cronin, 2018) eroding and delivering gravel *en masse* (Walker, 1975), and tractional reworking by turbidity currents (Cronin, 2018).

Non-cohesive granular debris flows may have originated from failure of oversteepened slopes and eroded the seafloor (Dakin *et al.*, 2013), resulting in steep truncation surfaces. Terrestrial granular debris flows have been documented to become channelised and build coarse-grained levees and frontal lobes (Kim & Lowe, 2004). Deposits attributed to similar processes have been identified in submarine settings (Sohn, 2000; Kane *et al.*, 2009). The sequence in Fig. 6h shows deposits that may have resulted from a propagation of a submarine debris flow. The mudclast-rich sandstone and mudclast breccia represent the excavation of a mud-rich substrate and an increase in flow cohesion. The gravel-sand cross-bedded wedge is then likely to be the frontal lobe, and the coarsest gravel cross-bedded interval represents the levee to the 1.5 m wide channel with a conglomeratic fill.

Tractional reworking of gravel on the canyon floor by overriding sediment gravity flows resulted in more organised, sorted, and structured conglomerate deposits. Conglomerate deposits developed pronounced clast imbrication in channel thalwegs, requiring sustained high flow velocities for bedload transport. Cross-bedded and well-sorted conglomerates or conglomerates-sandstones represent accretion surfaces of migrating mid-braid-plain or bank-attached bars (Klaucke & Hesse, 1996; Hesse *et al.*, 2001). Horizontally interstratified conglomerate-sandstone is formed by traction carpets (Lowe, 1982; Cronin, 2018). The metre-scale truncation surfaces represent scours filled by sand and gravel from subsequent flows.

Sandstone is generally underrepresented in braid plain deposits. This is attributed to the strongly bypassing nature of turbidity currents that likely reworked the gravel deposits. Turbidity currents that deposited sand and mud on the braid plain are preserved as scour-fills and channel margin deposits, which were shielded by their negative relief. Evidence for fine-grained deposition on the braid plain comes in the form of abundant sandstone rafts, mudclast-rich sandstones, and mudclast breccias found in axial deposits. These represent the erosional products of semi-lithified deposits, transported over limited transport distances.

4.2.2 AXIS – channel margin

Description: The channel margin facies association is up to 15 m thick and characterised by thick- to thin-bedded sandstones (ST), with heterolithics (H) and minor conglomerates (CSx). Commonly, beds are normally graded and stack in generally fining- and thinning-upwards successions, with decreasing bed amalgamation. The channel margin facies association typically overlies erosion surfaces that cut into braid plain deposits. Beds appear tabular in dip section, but in strike section generally thin and fine eastwards to onlap metre-scale westward-dipping truncation surfaces. Debrites may overlie these surfaces, which are in turn onlapped by sandstones of facies ST. Locally, these deposits are folded. Coarse-grained lag deposits or conglomerate beds are common at bed bases. Load-structures of conglomerate into sandstone are common, often planed-off and completely separated from conglomerate beds (Fig. 7b). Sandstones often display dewatering structures, such as pipes and load balls (Fig. 7g). Commonly, current ripple lamination is steeply climbing, with high amplitude and variable mud-content (Fig. 7i). Rippled beds generally indicate a south-east directed palaeoflow direction. Slumps, sandstone injections, mudclast breccia, and debrite deposits are common, in various stages of disaggregation (Fig. 6a,b; Fig. 7g). A thicker interval of amalgamated debrites and slumps is preserved in the north of the field area, with medium- to thick-bedded turbidites of this facies association onlapping mass transport relief, with common low-angle cross-bedding (Fig. 7c) and a variety of ripple types and palaeocurrent directions. Vertical paired *Tisoa* burrows are found in debrites below erosion surfaces.

Interpretation: We interpret this facies association as a channel margin setting within a channel belt in the accommodation formed by bank failure and erosion. These deposits formed in a transitional region between the axis and the overbank. Deposition was by turbidity currents lateral to the highest-energy parts of flows in the thalweg. Abundant de-watering structures and steeply climbing, high-amplitude ripples suggest high rates of deposition, with varying mud content in ripples indicating deposition under rapidly decelerating flows (Baas *et al.*, 2011; Taylor *et al.* In press). Energy was still occasionally high, evidenced by the detached conglomeratic load-balls (Fig. 7b) signifying high degrees of sediment bypass. As the topography healed, deposits thinned and fined upward as the bank was filled. The beds are (sub-)horizontal and there is no indication of lateral accretion, so these deposits do not represent lateral migration of open channels.

Low-angle cross-bedding observed in thick-bedded sandstones of this facies association is found near confining surfaces (cutbank, canyon wall, or mass transport deposit relief). This supports an interpretation of flow reflection and deflection off such a surface, combined with sustained supercritical flow, to result in low-angle cross-bedded thick beds (Slootman & Cartigny, 2020). The same flow-topography interaction is held responsible for the varying nature and migration direction of ripples in thinner-bedded turbidites near these confining surfaces (Edwards *et al.*, 1994; Taylor *et al.* In press). The denser, coarser-grained parts of flows that deposited the low-angle cross-bedded thick beds carried more momentum and were thus less affected by the topography than the more dilute, finer-grained parts of flows that deposited the ripple laminated thin-bedded turbidites.

4.2.3 OVERBANK

Description: The overbank facies association forms thin- to medium-bedded heterolithic successions with varying sandstone to mudstone ratios, with common upward bed thinning and increased mud-content. The overbank facies association commonly conformably overlies axial and channel margin deposits, or rarely is in sharp contact with slumped beds below. Medium-bedded sandstones form isolated outsized beds that may form positive relief, with dune-scale cross-bedding (Fig. 7e). Pebble-grade lag deposits (Fig. 7a) and flat-topped coarse sandstone to gravel lenses (Fig. 7f) occur sporadically, concentrated towards the western extent of this facies association. Bioturbation intensity is variable but generally high. Typically, sandstones (ST) are horizontally laminated to ripple cross-laminated. Ripple types include high-angle climbing, mixed grain-size (high-amplitude with mud-rich troughs and low amplitude), reversal (Fig. 7j), starved ripple trains (Fig. 7h), and starved lamination (Taylor *et al.*, 2023). Palaeocurrent directions are variable but with a tendency towards the south-east, with common opposing directions. Shallow-angle erosion surfaces are common and filled with sandstone (Fig. 7d).

Interpretation: We interpret this facies association as overbank deposits. The finer-grained, more dilute parts of turbidity currents are either flow stripped from, or overspill the main braid plain confinement to deposit thin-bedded turbidites, while the denser, more concentrated part of rare larger magnitude flows overspill the main braid plain confinement to deposit the thicker bedded and coarser-grained turbidites. Medium-bedded sandstone with dune-scale cross-bedding (Fig. 7e) within thin-bedded deposits implies out-sized flows depositing and tractionally reworking sand on the overbank (e.g. McArthur *et al.*, 2020; Soutter *et al.* In Press). Pebble lags (Fig. 7a) within thin-bedded turbidite successions imply a high-density traction flow winnowing, transporting, and bypassing in an otherwise low-density flow environment (Allen *et al.*, 2022a). Starved ripple lamination and laminae indicate that overbanking flows were occasionally sediment-starved. Local breaches of the main braid plain confinement result in crevasse-like deposits with a coarsening-up highly aggradational character, or develop high aspect ratio overbank channels represented by the flat-topped coarse-grained lenses (Fig. 7f). Complex facies distributions, scour surfaces (Fig. 7d), palaeocurrent patterns, and combined flow signatures (Fig. 7j) point to flow interaction with the canyon wall or other locally confining surfaces driving reflection and deflection (Kane et al. 2010). Mixed-grainsize transitional bedforms are common in this environment due to flows incorporating mud from the overbank or higher up on the canyon walls.

4.2.4 SHALLOW MARINE

Description: This facies association reaches up to 15 m thick and is dominated by thick-bedded sandstones and minor heterolithic deposits. The base is erosional and truncates channel margin or overbank deposits. This facies association is overlain by the El Gallo Formation beach boulder unconformity. Sandstone beds are dominantly low-angle cross-laminated, and commonly grade into symmetrically-rippled sandstone and thinly interbedded sandstones and mudstones. Siderite concretions and siderite-cemented *Ophiomorpha* and *Thalassinoides* burrows are common. Mudclast breccias are found in the thickest beds. Upward thinning trends are common. In one instance this is preceded by an upward thickening trend. Palynofacies consist of mixed opaques and Amorphous Organic Matter with poor recovery and poor preservation, and deposits are rich in *Gonylacoid* dinoflagellate cysts.

Interpretation: We interpret this facies association to represent restricted to shallow marine conditions. The low-angle cross-lamination in combination with the symmetrical ripples and siderite cement is typical of near-shore depositional environments (Reading, 1996). The upwards thickening-then-thinning trends likely represent the migration of shoreface bars. The ichnofacies and palynofacies agree with a more restricted environment compared to the deep-water deposits in the rest of the canyon fill. The detrital-Zircon-derived age and stratigraphic position of this facies association below the El Gallo Formation unconformity leads us to conclude that these are transgressive deposits, preserved below the main wave-ravinement surface of the El Gallo Formation, in the embayment that the Punta Baja canyon head likely formed at that time.

4.3 Architecture

The Punta Baja canyon-fill forms a 5 x 2 km exposure, mainly as coastal cliffs, with a general SW paleocurrent direction (Fig. 4). It incises the fluvial bedrock of the Bocana Roja Formation (Fig. 10a,b). This contact is exposed in multiple places around the peninsula.

We constructed three strike and one dip cross-sections by projecting field mapping and measured sections on DEM-derived topographic profiles, assisted by virtual outcrop models. The chosen strike sections provide different stratigraphic windows into the canyon fill succession with X3 the stratigraphic lowest and X1 the highest (Fig. 9).

Canyon wall

The steep erosional contact between the Bocana Roja Formation bedrock and the Punta Baja Formation canyon-fill is well exposed along the eastern and western sides of the peninsula. The canyon wall erosion surface in the east truncates fluvial floodplain deposits and braided stream conglomerates (Fig. 10a,b), and is overlain by mud-rich mass transport and overbank heterolithic deposits of the canyon fill (Fig. 9, Fig. 10f). The western canyon wall truncates floodplain deposits of the Bocana Roja Formation and is overlain by a broad variety of canyon fill facies, but dominantly conglomerates (Fig. 10c,d,e). Locally, the canyon wall is scalloped and overlain by chaotic facies, representing slide scars, chutes, and gullies shaping the canyon margin. In the west, these scallop surfaces are filled with dark pebbly mudstone and thin-bedded turbidites steeply onlapping the contact (Fig. 10d). In the east, a conglomeratic and coarse sand-filled scallop overlies the canyon wall, in an otherwise thin-bedded depositional environment.

Overall, the eastern margin is dominantly overlain by channel margin and overbank deposits, and the western margin by axial conglomerates. A notable exception is on the western side of the peninsula, where a 10 m-thick interval with a wide variety of facies is found overlying the canyon wall (Fig. 11). Irregular canyon wall topography, such as terrace surfaces could have facilitated the range of depositional conditions that lead to the wide variety of facies onlapping the canyon wall in this location.

Lower fill

The lowermost exposed canyon fill is dominated by unorganized and poorly sorted conglomerates containing large (~4 m diameter) angular blocks of red sandstone from the Bocana Roja Formation bedrock (Fig. 12a,c) signifying ongoing canyon wall excavation during canyon fill. Within these chaotic conglomerates sit sand-prone scour- and channel-fills with complex cross-cutting relationships and pebble-lined bypass surfaces (Fig. 12b,d). These relationships are interpreted as braid plain deposits that accumulated during the initial high-energy filling of the canyon, (Fig. 12a).

Upper fill

Braid plain deposits in the eastern canyon fill are overlain by, and laterally interfinger with mud-rich debrites with contorted thin bedded turbidites (Fig. 9). The conglomerates at the base are steeply truncated towards the west. The N-S oriented truncation surface is overlain by deformed turbidites and rotationally slumped thick-bedded channel margin deposits. The failure direction as indicated by slump vergence is to the west, perpendicular to the truncation surface (Fig. 9). These slumps grade towards the west into axial braid plain deposits, and are overlain by thick-bedded channel margin turbidites. The preservation of the channel margins means that the thalweg, which would normally cannibalise these deposits, migrated outward. A westward migration of the channel belt is indirectly recorded by the preservation of multiple cutbank surfaces and fills (Fig. 13). This geometry and process interpretation is akin to the “lateral step remnants” proposed by Kane et al. (2010), to differentiate such deposits from true lateral accretion.

Finer-grained overbank material is preserved mainly on the eastern canyon margin, with conglomeratic braid plain deposits vertically stacking and amalgamating along the western canyon margin. Generally, overbank deposits thin- and fine-upwards, with a similar eastward trend in the upper canyon fill. A thick (<10 m) interval of channel margin deposits is preserved along the western side of the field area, bounded by conglomeratic braid plain deposits below and above. West- to southwest-oriented conglomerate-filled scour surfaces truncate thick-bedded sandstone channel margin deposits (Fig. 6e), and in most places amalgamate with underlying conglomeratic braid plain deposits.

Mass transport deposits

In the northern, most upstream part of the field area, the sand-rich channel margin deposits are overlain by and interbedded with mud-rich debrites and slumps. Their mud-rich or thin-bedded composition supports a source from the unstable canyon wall. Sandstone lenses intercalated with the debrites and slumps display erosive to conformable bases with multi-directional fanning geometries (Fig. 14d) and a general thinning- and fining-upwards trend. Complex paleocurrent patterns in ripples and low-angle cross-bedding indicate abundant flow reflection and deflection. The *Tisoa* burrows below erosion surfaces indicate that conduits were active and open above these mass transport deposits (Knaust, 2019). We interpret this succession as representing multiple mass wasting events with sandstones foundering above, and channels navigating across, mass transport relief.

Up-flow dipping surfaces

Generally, sedimentary surfaces within the axial conglomerates of the Punta Baja canyon-fill are steeper than bedding surfaces in sandstone or heterolithic deposits. The steepness of these surfaces, whether resulting from erosion or deposition, was maintained due to the conglomerates, which increases the angle of repose and stability of the seabed compared to their sand-rich equivalents. Due to the extensive dip-exposure of axial canyon deposits in the field area, we can document for the first time in outcrop the spatial extent and 3D orientation of the main canyon-fill building surfaces. The orientation of these surfaces is related to flow processes on multiple scales. Small-scale scours can form complicated 3 dimensional surfaces.

Therefore, only larger-scale planar surfaces are included in the analysis, and concave or convex erosional scours and dune-scale bedforms are excluded.

The scale of the measured surfaces exceeds the bed scale with a mean measured plane diameter of 10.2 m, and a mean dip of 12.7°. Most surfaces are upstream-inclined, with a mean dip direction to the ENE, nearly opposite the mean flow direction to the SW (Fig. 15). This preferred upstream orientation is not caused by post-depositional tectonic tilting, since surfaces generally dip more steeply (76.7% between 5 - 30°) than the structural tilt (<5°) of the Punta Baja Formation. Moreover, the structural tilt is southward, which should cause overrepresentation of downstream dipping surfaces.

Whereas upstream dipping surfaces clearly dominate over downstream, flow-perpendicular orientations show a slight tendency to the SE. This variability is probably caused by local variations in axis thalweg direction, more sinuous braid plain channel planforms, and outcrop orientation to a lesser degree.

El Gallo unconformity

The nature of the contact with the overlying El Gallo Formation is variable, consisting of yellow-weathering shallow marine deposits or a very well-rounded bored-boulder lag with a white matrix (Fig. 16a), which locally is preceded by red-weathering matrix-supported gravels with angular clasts (Fig. 16b). The age of these shallow marine deposits as indicated by detrital zircon dating (78.5±0.9 Ma), is younger than other canyon-fill deposits (min. 80.8±1.0 Ma), but also older than El Gallo Formation (max. 72.3±0.5 Ma) samples in the area (Fig. 9; Supplementary materials). Micropaleontological samples suggest an open, but relatively restricted marine setting.

5 Discussion

5.1 Canyon evolution

5.1.1 Incision to fill

Our structural data demonstrates that the Punta Baja canyon is aligned with the structural fabric of the bedrock (Fig. 4), in agreement with Kane et al. (2022). This localised expression of the regional stress regime that caused subsidence formed a relatively minor structural depression that was enough to divert submarine sediment gravity flows from the regional west-dipping slope (Fig. 17 t1). Initial capturing and focusing of sediment gravity flows enhanced erosion of the bedrock and promoted incision and deepening of the nascent canyon (Fig. 17 t2). Scallop-shaped erosion surfaces on the canyon wall overlain by chaotic facies representing slide scars, chutes, and gullies coincide with bedrock faults. A sand-rich canyon wall gully-fill on the eastern canyon margin suggests that smaller lateral conduits transferred sediment from the shelf into the canyon, in this case depositing outsized sediment to the overbank environment. The lowermost canyon fill, comprising chaotic conglomeratic deposits with abundant clasts from the adjacent bedrock (Fig. 12), represent coarse-grained lag deposits and a sediment bypass-dominated period (Stevenson *et al.*, 2015). Overall, this phase of canyon formation was dominated by erosion, sediment bypass, and canyon wall failure.

5.1.2 Early fill

During the incisional phase, dilute parts of bypassing turbidity currents ran up the canyon wall to deposit fine-grained thin-bedded turbidites above the irregular topography of the canyon margins (Fig. 10d). Accumulations of thin-bedded turbidites could have been remobilised, resulting in the mud-rich mass transport deposits in the Punta Baja canyon-fill. Lateral canyon wall failure caused instantaneous widening of confinement, allowing passing flows to expand and become depositional. The mass transport deposits formed topographic barriers to flows (Fig. 17 t3). Multiple phases of mass transport deposition and canyon floor aggradation could have been entirely eroded while the highly energetic canyon was deepening. However, the combination of instantaneous canyon widening and decreased thalweg gradient due to mass transport deposition, promoted the (local) onset of canyon floor aggradation.

5.1.3 Aggradational fill

The preservation of overbank material on the eastern margin marks the aggradational stage of the canyon fill. As the canyon filled and the floor became elevated and thus wider, flows focused in an axial thalweg were stripped and overspilled onto the overbank. Erosional entrenchment of the thalweg could have forced lateral flow segregation due to the elevation difference between the lower high-density and upper low-density parts of stratified flows. Mass transport deposits also formed superelevated relief above the thalweg. Thus, flow stripping and overspill from the thalweg confinement constructed local overbank successions. Our field observations (Fig. 9 X3) suggest a strong link between the emplacement and preservation of mass transport deposits and onset of overbank accumulation (Fig. 17 t4).

Axial thalweg migration is recorded by westward-cutting-and-aggrading channel margin deposits, grading eastwards and upwards into thin-bedded overbank deposits (Fig. 13). The canyon-fill asymmetry suggests that, overall, the axis migrated westward, contributing to the upwards fining and thinning trend on the eastern overbank area.

This asymmetry may be attributed to tectonic releasing bend characteristics, with the centre of active extensional tectonism stepping north and westward through time. Other contributing factors for the architectural asymmetry could have been the regional westward sloping basin margin and the pinning of a sinuous channel outer bend (Brunt *et al.*, 2013). Rotational slumping of eastern channel margin deposits (Fig. 9 x3) supports that active incision was focused on the western margin of the canyon.

Thalweg widening followed by entrenchment, and pulses of eastward thalweg migration, and/or bank erosion result in remnants of lateral steps on the eastern side of the thalweg (Fig. 13), when axis migration resumed its general westward tendency (Fig. 17 t4). The repeated bank cutting, and gradual accretion of the channel margin and overbank suggests that the canyon was an active conduit for flows that transported and partially bypassed a wide range of grainsizes during filling.

The thick accumulation of channel margin deposits can represent 1) a westward migration of the canyon axis, with laterally equivalent braid plain deposits now eroded beyond the western coastline, or 2) a decrease in grainsize delivered to these reaches of the canyon, resulting in sand-rich channel systems filling the canyon thalweg. The latter could be caused by an upstream intra-canyon blockade trapping the gravel fraction, a relative sea level rise after which the sediment delivery had to re-adjust, or a change in sediment supply from the hinterland drainage system. The presence of gravel lags in the channel margin deposits supports a more western axis with its conglomeratic braid plain deposits unexposed.

Continued erosion caused canyon wall failure and the emplacement of a thick succession of mass transport deposits in the canyon axis. Flows were diverted or partially blocked by the positive relief of these mass transport complexes (Fig. 17 t5). When gravity flows eventually overcame the depositional relief, the canyon thalweg re-established in a more eastward (canyon-central) position, incising into the mass transport deposit and underlying channel margin deposits.

This net-aggradational phase of canyon development shows evidence of a highly efficient conduit, that eroded and bypassed sediment in an entrenched axis, while an overbank aggraded. The conglomeratic axial fill with sandstone-filled scours suggests that flows bypassed grainsizes up to pebble/cobble through the axis, with the higher, sand- and mud-bearing parts of flows partially stripping and spilling onto the overbank. The abundant erosional structures, coarse-grained lags, and down-canyon palaeocurrent directions in the overbank deposits suggest that even bank-overspilling flows underwent a high degree of down-canyon bypass.

5.1.4 Late fill

No stratigraphic evidence remains for further stages of canyon evolution, owing to the El Gallo Formation ravinement unconformity However, the more restricted or shallow marine character of the early El Gallo Formation deposits suggests deposition in a shelf-incised embayment. This constrains the proximal position and short sediment transport distance of the Punta Baja submarine canyon deposits relative to its head on the steep basin margin.

5.2 Unique sedimentary properties of submarine canyons and their stratigraphic character

5.2.1 Flows interacting with dynamic topography caused by mass wasting

Mass transport deposits in the Punta Baja canyon fill are common and are shown to impact canyon sedimentation and erosion patterns profoundly. The restoration of channel gradients across mass transport deposits has at least partially been attributed to upstream migrating knickpoints or knickpoint zones (Tek *et al.*, 2021; Allen *et al.*, 2022b). The increased gradient on the downstream part of the mass transport deposits is likely to induce knickpoints, that incise headward across the mass transport deposit and produce steep, stepped, and composite erosion surfaces (Allen *et al.*, 2022b). These may be infilled with coarse-grained and fining-up terrace deposits, or channelised sandstones. We observe foundering sandstone deposits on the mass transport complex relief (Fig. 14), indicating that sand-bearing parts of flows surmounted the mass transport relief (e.g. Martínez-Doñate *et al.*, 2021). Pebbles and cobbles were likely trapped behind the mass transport complex relief, as is observed in the modern Congo Canyon (Pope *et al.*, 2022). Where the surmounting sand-rich flows accelerated over the steep downstream part of the mass transport complex, knickpoints or knickpoint zones could be initiated. Indeed, we find erosion surface-bound fining-up sandstone successions (<5 m thick) within and near the top of the mass transport complex (Fig. 14), which could record deposition directly downstream of a migrating knickpoint. When these knickpoints, knickpoint zones, or sand-rich channels were able to connect across the mass transport deposit, a conduit was re-established and gravel transport was resumed, evidenced by the return of conglomeratic axis deposits (Fig. 14)

The erosion by knickpoints and channels into the mud-rich mass transport deposits would have resulted in increased mud-content of flows, leading to mud-rich transitional flows downstream. The erosion rates due to knickpoint migration could also be instrumental in providing the near-bed sediment concentrations that are necessary for the development and migration of backsets (Englert *et al.*, 2023), that produced the upstream inclined surfaces (Fig. 15).

The dynamic erosional and depositional relief caused by mass wasting events is thus a main factor in sediment capture and storage in submarine canyons, modifying downstream sediment delivery patterns and possibly overriding allogenic input signals.

5.2.2 The impact of proximal position on transverse flow filtering

The Punta Baja canyon fill stratigraphy has abundant large-scale erosion surfaces and thick, chaotic conglomerates (Fig. 6). This duality suggests an environment where large-scale catastrophic events eroded as well as deposited. Proximity to the canyon head could play an important role in the described stratigraphic expression of gravity flow activity and magnitude. The canyon head can act as a sediment 'capacitor', storing sediment until catastrophic failure discharges large volumes of sediment down-canyon (Clare *et al.*, 2016; Bailey *et al.*, 2021; Talling *et al.*, 2023). The regions of sediment buffering thus experience different patterns of erosion and deposition than their down-system reaches. The position and extent of this region changes as the canyon evolves, shifting upstream in the case of a retrogressive canyon head. Other structures in canyons may have similar sediment buffering and discharging effects, such as landslide dams (Pope *et al.*, 2022) or faults (Mountjoy *et al.*, 2009; Micallef *et al.*, 2014), which have a less predictable spatial and stratigraphic trajectory than canyon heads. Stratigraphic evidence of this temporary sediment buffering will be inherently difficult to identify, due to the catastrophic erosional nature of the collapsing buffer. Our dataset contains the downstream expression of large-magnitude canyon-flushing flows that likely originated by failure in the canyon head, in the form of large-scale erosion surfaces and *en masse* deposited conglomerates.

Overbank deposits in the Punta Baja canyon display a wider range of grain sizes and bed thicknesses, with a less predictable character, compared to more distal deep-water thin bed successions like external levees. Submarine canyon reaches are in a unique position where gravity flows may either deposit up dip of leveed channels, or are yet to bulk up and travel great distances (Heijnen *et al.*, 2022a). Flows through canyons are thus rarely in equilibrium with the canyon gradient and intra-canyon confinement, contrary to lower slope and basin floor settings. This lack of filtering means that overbank deposits within submarine canyon fills should provide a more complete record of events than downstream external levee or basin-floor lobe successions. However, the record in submarine canyon environments is subject to regular and severe erosion and reworking, resulting in an incomplete record. The near-constant disequilibrium between flows and bank confinement in canyons prevents the development of an organised overbank that is reported in external levees (e.g. Kane & Hodgson, 2011). The resulting lack of transverse flow filtering is reflected in our dataset by the wide range and unpredictable nature of grain sizes and bed thicknesses in overbank deposits within canyons.

5.3 Comparison to the Monterey canyon

Nine hundred and forty kilometres north of Punta Baja, along the same Pacific coast transform margin, lies the modern Monterey Canyon. The Monterey canyon has been studied since the early 20th century (Beal, 1915), with recent pioneering direct monitoring studies (e.g. Smith *et al.*, 2007; Xu & Noble, 2009; Symons *et al.*, 2017; Paull *et al.*, 2018; Maier *et al.*, 2019; Bailey *et al.*, 2021) that have advanced our understanding of modern canyon sediment transport processes. The Monterey submarine canyon system consists of an active canyon-fan on the present-day seafloor, and ancient remnant fills that have been imaged in the subsurface (Fig. 18)(Maier *et al.*, 2018). The entire grainsize range from clay to cobbles is found on the modern canyon floor, with powerful flows regularly passing though. The similarities in tectonic setting and grainsize range means that the Monterey canyon represents a modern analogue to the Punta Baja canyon-fill.

A seismic reflection cross section through the upper reaches of the Monterey canyon (Fig. 18) reveals buried incision surfaces and asymmetric paleochannel fills, strikingly similar in scale and architecture to the Punta Baja canyon fill. It is worth noting that the present-day Monterey canyon incision is deeper and wider than both the Punta Baja canyon fill and most buried palaeocanyon fills in Monterey Bay. This implies that the preserved fill of a canyon might represent only a fraction of the true dimensions of the open conduit. The Punta Baja canyon-fill might thus represent a smaller incision and fill on a larger composite system-bounding surface that has been abandoned, re-occupied, and ultimately mostly removed by the El Gallo Formation unconformity. Alternatively, the Punta Baja canyon might have been a tributary canyon to a larger system now not exposed.

The abundant re-incisions and amalgamation in the seismic section highlight the complexity of lateral and vertical facies relationships in canyon fills. If exposure, detail, or contrast is limited, the nature of erosion surfaces may be deceiving; a subtle erosion surface might in fact represent a much younger re-incision, instead of a time-equivalent facies transition. In the Punta Baja canyon fill we can be reasonably certain that the axial braid plain and overbank were pene-contemporaneous due to good lateral control, despite facies transitions are generally erosion-bounded. The timing of establishment of the upper conglomeratic axis deposition is unlikely to represent a prolonged abandonment and re-incision of the canyon, as the foundered sandstones within the mass transport complex indicate continuous sediment throughput. The erosion surfaces at the base of major facies changes appear to have truncated semi-soft deposits, further evidencing continuous activity.

6 Conclusions

In the area of Punta Baja a bedrock incised submarine canyon, with an asymmetric coarse-grained axial fill and finer-grained intra-canyon overbank deposits is exposed. The structural and stratigraphic evolution of the Punta Baja submarine canyon is reconstructed from incision to fill:

- An inherited tectonic fabric influenced the location and orientation of canyon incision into fluvial bedrock.
- The depositional architecture of the north-south oriented erosionally confined canyon-fill is asymmetric, with sub-vertically stacked channel-fills to the west, and an overbank confined by the canyon margin in the east.

Sedimentary process interactions led to depositional patterns that we consider distinct to submarine canyon fills:

- Dynamic topography created by mass wasting processes captured sediment and drove knickpoint development, an autogenic mechanism that modifies sediment delivery to the ocean floor.
- We interpret widespread upstream dipping surfaces in channel-fills as the stratigraphic expression of migrating supercritical-flow bedforms, playing an important role in sediment storage and transport in the canyon.
- The proximal location of canyons and unique confinement configuration impact transverse and lateral gravity flow filtering, causing depositional patterns, including scours and bypass lags, in the intra-canyon overbank areas that are less well organised than in published examples of external levees and which were previously poorly characterised for submarine canyons.
- The canyon remained an active sediment conduit throughout the time period represented by the preserved fill.

This study provides insight into how processes that are observed in modern canyons are selectively preserved through the lifetime of the canyon and construct or destroy stratigraphy on geological timescales.

Acknowledgements

We thank Steve Hubbard and his group at the University of Calgary for enabling the Detrital Zircon analysis and Julia Drummond for performing the laboratory analysis. This study is part of the Slope5 JIP, made possible by our sponsors (AkerBP, BP, CNOOC, Hess, Murphy, Neptune, Petrobras, Vär, Woodside, Wintershal Dea).

Data availability statement

The data that supports the findings of this study are available in the supplementary material of this article.

7 References

Advocate, D.M., **Link, M.H.** and **Squires, R.L.** (1988) Anatomy and History of an Eocene Submarine Canyon: the Maniobra Formation, Southern California. In: *Paleogene Stratigraphy, West Coast of North America* (Ed. M.V. Filewicz and R.L. Squires), *Pacific Section, SEPM*, 45–58.

Allen, C., **Gomis-Cartesio, L.E.**, **Hodgson, D.M.**, **Peakall, J.** and **Milana, J.** (2022a) Channel incision into a submarine landslide on a Carboniferous basin margin, San Juan, Argentina: Evidence for the role of knickpoints. Depos Rec. doi: 10.1002/dep2.178

Allen, C., **Gomis-Cartesio, L.E.**, **Hodgson, D.M.**, **Peakall, J.** and **Milana, J.** (2022b) Channel incision into a submarine landslide on a Carboniferous basin margin, San Juan, Argentina: Evidence for the role of knickpoints. *Depos. Rec.*, 1–28.

Allen, S.E. and **Durrieu De Madron, X.** (2009) A review of the role of submarine canyons in deep-ocean exchange with the shelf. *Ocean Sci.*, **5**, 607–620.

Allmendinger, R.W., **Cardozo, N.** and **Fischer, D.M.** (2013) Structural Geology Algorithms: Vectors and Tensors. *Cambridge University Press*, Cambridg.

Almgren, A.A. and **Hacker, P.D.** (1984) Paleogene Submarine Canyons of The Sacramento Valley, California. *Pacific Section American Association of Petroleum Geologists*.

Alsleben, H., **Wetmore, P.H.**, **Gehrels, G.E.** and **Paterson, S.R.** (2012) Detrital zircon ages in Palaeozoic and Mesozoic basement assemblages of the Peninsular Ranges batholith, Baja California, Mexico: Constraints for depositional ages and provenance. *Int. Geol. Rev.*, **54**, 93–110.

Aslam, T., **Hall, R.A.** and **Dye, S.R.** (2018) Internal tides in a dendritic submarine canyon. *Prog. Oceanogr.*, **169**, 20–32.

Azpiroz-Zabala, M., **Cartigny, M.J.B.**, **Talling, P.J.**, **Parsons, D.R.**, **Sumner, E.J.**, **Clare, M.A.**, **Simmons, S.M.**, **Cooper, C.** and **Pope, E.L.** (2017) Newly recognized turbidity current structure can explain prolonged flushing of submarine canyons. Sci Adv. doi: 10.1126/sciadv.1700200

Baas, J.H., **Best, J.L.** and **Peakall, J.** (2011) Depositional processes, bedform development and hybrid bed formation in rapidly decelerated cohesive (mud–sand) sediment flows. *Sedimentology*, **58**, 1953–1987.

Bailey, L.P., **Clare, M.A.**, **Rosenberger, K.J.**, **Cartigny, M.J.B.**, **Talling, P.J.**, **Paull, C.K.**, **Gwiazda, R.**, **Parsons, D.R.**, **Simmons, S.M.**, **Xu, J.**, **Haigh, I.D.**, **Maier, K.L.**, **Mcgann, M.**, **Lundsten, E.** and **Team, M.C.** (2021) Preconditioning by sediment accumulation can produce powerful turbidity currents without major external triggers. *Earth Planet. Sci. Lett.*, **562**, 116845.

Balster-Gee, A.F., **Maier, K.L.**, **Brothers, D.S.**, **Johnson, S.Y.**, **Hart, P.E.** and **Hartwell, S.R.** (2018) Multichannel minisparker seismic-reflection data of field activity 2015-617-FA; Monterey Bay, offshore central California from 2015-02-23 to 2015-03-06.

Beal, C.H. (1948) Geology and Oil Possibilities of Baja California.

Beal, C.H. (1915) The geology of the Monterey quadrangle, California. Stanford University

Bianchelli, S., **Gambi, C.**, **Zeppilli, D.** and **Danovaro, R.** (2010) Metazoan meiofauna in deep-sea canyons and adjacent open slopes: A large-scale comparison with focus on the rare taxa. *Deep Sea Res. Part I Oceanogr. Res. Pap.*, **57**, 420–433.

Boehlke, J.E. and **Abbott, P.L.** (1986) Punta Baja Formation, A Campanian Submarine Canyon Fill, Baja California, Mexico. In: *Cretaceous Stratigraphy Western North America: Los Angeles, Pacific Section* (Ed. P.L. Abott), *Society for Economic Paleontologists and Mineralogists*, Book 46, 91–101.

Boulesteix, K., **Poyatos-Moré, M.**, **Flint, S.S.**, **Taylor, K.G.**, **Hodgson, D.M.** and **Hasiotis, S.T.** (2019) Transport and deposition of mud in deep-water environments: Processes and stratigraphic implications. *Sedimentology*, **66**, 2894–2925.

Brunt, R.L., **Hodgson, D.M.**, **Flint, S.S.**, **Pringle, J.K.**, **Di Celma, C.**, **Prélat, A.** and **Grecula, M.** (2013) Confined to unconfined: Anatomy of a base of slope succession, Karoo Basin, South Africa. *Mar. Pet. Geol.*, **41**, 206–221.

Buckley, S.J., **Ringdal, K.**, **Naumann, N.**, **Dolva, B.**, **Kurz, T.H.**, **Howell, J.A.** and **Dewez, T.J.B.** (2019) LIME: Software for 3-D visualization, interpretation, and communication of virtual geoscience models. *Geosphere*, **15**, 222–235.

Busby, C.J. (2004) Continental growth at convergent margins facing large ocean basins: A case study from Mesozoic convergent-margin basins of Baja California, Mexico. *Tectonophysics*, **392**, 241–277.

Busby, C.J., **Fackler Adams, B.**, **Mattinson, J.** and **Deoreo, S.** (2006) View of an intact oceanic arc, from surficial to mesozonal levels: cretaceous Alisitos arc, Baja California. *J. Volcanol. Geotherm. Res.*, **149**, 1–46.

Busby, C.J., **Smith, D.**, **Morris, W.** and **Fackler-Adams, B.** (1998) Evolutionary model for convergent margins facing large ocean basins: Mesozoic Baja California, Mexico. *Geology*, **26**, 227–230.

Cardozo, N. and **Allmendinger, R.W.** (2013) Spherical projections with OSXStereonet. *Comput. Geosci.*, **51**, 193–205.

Christie-Blick, N. and **Biddle, K.T.** (1985) Deformation and Basin Formation along Strike-Slip Faults. In: *Strike-Slip Deformation, Basin Formation, and Sedimentation* (Ed. K.T. Biddle and N. Christie-Blick), *SEPM (Society for Sedimentary Geology)*, 1–34.

Clare, M., **Hunt, J.**, **Kane, I.**, **Fonnesu, M.**, **Malgesini, G.** and **Bailey, L.** (2023) Instability of deep-sea currents over tidal and seasonal timescales. 1–19 pp.

Clare, M.A., **Hughes Clarke, J.E.**, **Talling, P.J.**, **Cartigny, M.J.B.** and **Pratomo, D.G.** (2016) Preconditioning and triggering of offshore slope failures and turbidity currents revealed by most detailed monitoring yet at a fjord-head delta. *Earth Planet. Sci. Lett.*, **450**, 208–220.

Cronin, B.T. (2018) Lithofabric classification and distribution of coarse-grained deep-water clastic depositional systems. In: *Rift-related coarse-grained submarine fan reservoirs; the Brae Play, South Viking Graben, North Sea: AAPG Memoir 115* (Ed. C.C. Turner and B.T. Cronin), 39–96.

Dakin, N., **Pickering, K.T.**, **Mohrig, D.** and **Bayliss, N.J.** (2013) Channel-like features created by erosive submarine debris flows: Field evidence from the Middle Eocene Ainsa Basin, Spanish Pyrenees. *Mar. Pet. Geol.*, **41**, 62–71.

Daly, R.A. (1936) Origin of submarine canyons. *Am. J. Sci.*, **31**, 401–420.

Dasgupta, S. and **Buatois, L.A.** (2015) High-frequency stacking pattern and stages of canyon / gully evolution across a forced regressive shelf-edge delta-front. *Mar. Pet. Geol.*, **68**, 40–53.

Di Celma, C. and **Cantalamessa, G.** (2012) Off-shelf sedimentary record of recurring global sea-level changes during the Plio-Pleistocene: evidence from the cyclic fills of exhumed slope systems in central Italy. *J. Geol. Soc. London.*, **169**, 643–646.

Dickinson, W.R. and **Gehrels, G.E.** (2009) U-Pb ages of detrital zircons in Jurassic eolian and associated sandstones of the Colorado Plateau: Evidence for transcontinental dispersal and intraregional recycling of sediment. *Geol. Soc. Am. Bull.*, **121**, 408–433.

Dickinson, W.R. and **Lawton, T.F.** (2001) Carboniferous to Cretaceous assembly and fragmentation of Mexico. *Bull. Geol. Soc. Am.*, **113**, 1142–1160.

Edwards, D.A., **Leeder, M.R.**, **Best, J.L.** and **Pantin, H.M.** (1994) On experimental reflected density currents and the interpretation of certain turbidites. *Sedimentology*, **41**, 437–461.

Englert, R.G., **Vellinga, A.J.**, **Cartigny, M.J.B.**, **Clare, M.A.** and **Eggenhuisen, J.T.** (2023) Controls on upstream-migrating bed forms in sandy submarine channels. *Geology*, 1–6.

Fastovsky, D.E., **Montellano-ballesteros, M.**, **Fricke, H.C.**, **Ramezani, J.**, **Tsukui, K.**, **Wilson, G.P.**, **Hall, P.**, **Hernandez-Rivera, R.** and **Alvarez, G.** (2020) Paleoenvironments, taphonomy, and stable isotopic content of the terrestrial, fossil-vertebrate–bearing sequence of the El Disecado Member, El Gallo Formation, Upper Cretaceous, Baja California, México. *Geosphere*, **16**, 1–21.

Fernandez-Arcaya, U., **Ramirez-Llodra, E.**, **Aguzzi, J.**, **Allcock, A.L.**, **Davies, J.S.**, **Dissanayake, A.**, **Harris, P.**, **Howell, K.**, **Huvenne, V.A.I.**, **Macmillan-Lawler, M.**, **Martín, J.**, **Menot, L.**, **Nizinski, M.**, **Puig, P.**, **Rowden, A.A.**, **Sanchez, F.** and **Van den Beld, I.M.J.** (2017) Ecological role of submarine canyonsand need for canyon conservation: A review. *Front. Mar. Sci.*, **4**, 1–26.

Fildani, A. (2017) Submarine Canyons: A brief review looking forward. *Geology*, **45**, 383–384.

Fisher, W.L., **Galloway, W.E.**, **Steel, R.J.**, **Olariu, C.**, **Kerans, C.**, **Mohrig, D.**, **Fisher, W.L.**, **Galloway, W.E.** and **Steel, R.J.** (2021) Deep-water depositional systems supplied by shelf-incising submarine canyons: Recognition and significance in the geologic record. Earth Sci Rev. doi: 10.1016/j.earscirev.2021.103531

Galloway, W.E., **Dingus, W.F.** and **Paige, R.E.** (1991) Seismic and Depositional Facies of Paleocene-Eocene Wilcox Group Submarine Canyon Fills, Northwest Gulf Coast, U.S.A. In: *Seismic Facies and Sedimentary Processes of Submarine Fans and Turbidite Systems* (Ed. P. Weimer and M.H. Link), *Frontiers in Sedimentary Geology*, 247–271.

Gastil, R.G., **Phillips, R.P.** and **Allison, E.C.** (1975) Reconnaissance Geology of the State of Baja California. *Geol. Soc. Am. Mem.*, **140**, 1–201.

Gastil, R.G., **Phillips, R.P.** and **Allison, E.C.** (1971) Reconnaissance geologicmap of the State of Baja California, scale 1:250 000. *Mem. Geol. Soc. Am.*, **140**, 179.

Hage, S., **Galy, V.V.**, **Cartigny, M.J.B.**, **Acikalin, S.**, **Clare, M.A.**, **Gröcke, D.R.**, **Hilton, R.G.**, **Hunt, J.E.**, **Lintern, D.G.**, **McGhee, C.A.**, **Parsons, D.R.**, **Stacey, C.D.**, **Sumner, E.J.** and **Talling, P.J.** (2020) Efficient preservation of young terrestrial organic carbon in sandy turbidity-current deposits. Geology. doi: 10.1130/G47320.1

Hagstrum, J.T., **McWilliams, M.**, **Howell, D.G.** and **Gromme, S.** (1985) Mesozoic paleomagnetism and northward translation of the Baja California Peninsula. *Geol. Soc. Am. Bull.*, **96**, 1077–1090.

Harris, P.T., **Macmillan-Lawler, M.**, **Rupp, J.** and **Baker, E.K.** (2014) Geomorphology of the oceans. *Mar. Geol.*, **352**, 4–24.

Heijnen, M.S., **Clare, M.A.**, **Cartigny, M.J.B.**, **Talling, P.J.**, **Hage, S.**, **Pope, E.L.**, **Bailey, L.**, **Sumner, E.**, **Gwyn Lintern, D.**, **Stacey, C.**, **Parsons, D.R.**, **Simmons, S.M.**, **Chen, Y.**, **Hubbard, S.M.**, **Eggenhuisen, J.T.**, **Kane, I.** and **Hughes Clarke, J.E.** (2022a) Fill, flush or shuffle: How is sediment carried through submarine channels to build lobes? *Earth Planet. Sci. Lett.*, **584**, 1–14.

Heijnen, M.S., **Mienis, F.**, **Gates, A.R.**, **Bett, B.J.**, **Hall, R.A.**, **Hunt, J.**, **Kane, I.A.**, **Pebody, C.**, **Huvenne, V.A.I.**, **Soutter, E.L.** and **Clare, M.A.** (2022b) Challenging the highstand-dormant paradigm for land-detached submarine canyons. *Nat. Commun.*, **13**, 3448.

Hesse, R., **Klaucke, I.**, **Khodabakhsh, S.**, **Piper, D.J.W.** and **Ryan, W.B.F.** (2001) Sandy submarine braid plains: Potential deep-water reservoirs. *Am. Assoc. Pet. Geol. Bull.*, **85**, 1499–1521.

Hsieh, Y., **Liu, C.**, **Suppe, J.**, **Byrne, T.B.** and **Lallemand, S.** (2020) The Chimei Submarine Canyon and Fan: A Record of Taiwan Arc-Continent Collision on the Rapidly Deforming Overriding Plate. Tectonics. doi: 10.1029/2020TC006148

Huang, L. and **Liu, C.Y.** (2017) Three Types of Flower Structures in a Divergent-Wrench Fault Zone. *J. Geophys. Res. Solid Earth*, **122**, 10,478-10,497.

Ito, M., **Ishikawa, K.** and **Nishida, N.** (2014) Distinctive erosional and depositional structures formed at a canyon mouth: A lower Pleistocene deep-water succession in the Kazusa forearc basin on the Boso Peninsula, Japan. *Sedimentology*, **61**, 2042–2062.

Janocko, J. and **Basilici, G.** (2021) Architecture of coarse-grained gravity flow deposits in a structurally confined submarine canyon (late Eocene Tokaren Conglomerate, Slovakia). *Sediment. Geol.*, **417**, 105880.

Johnson, S.E., **Tate, M.C.** and **Fanning, C.M.** (1999) New geologic mapping and SHRIMP U-Pb zircon data in the Peninsular Ranges batholith, Baja California, Mexico: Evidence for a suture? *Geology*, **27**, 743–746.

Kamb, W.B. (1959) Ice petrofabric observations from Blue Glacier, Washington, in relation to theory and experiment. *J. Geophys. Res.*, **64**, 1891–1909.

Kane, I.A., **Catterall, V.**, **McCaffrey, W.D.** and **Martinsen, O.J.** (2010a) Submarine channel response to intrabasinal tectonics: The influence of lateral tilt. *Am. Assoc. Pet. Geol. Bull.*, **94**, 189–219.

Kane, I.A., **Dykstra, M.L.**, **Kneller, B.C.**, **Tremblay, S.** and **McCaffrey, W.D.** (2009) Architecture of a coarse-grained channel-levée system: The Rosario Formation, Baja California, Mexico. *Sedimentology*, **56**, 2207–2234.

Kane, I.A. and **Hodgson, D.M.** (2011) Sedimentological criteria to differentiate submarine channel levee subenvironments: Exhumed examples from the Rosario Fm. (Upper Cretaceous) of Baja California, Mexico, and the Fort Brown Fm. (Permian), Karoo Basin, S. Africa. *Mar. Pet. Geol.*, **28**, 807–823.

Kane, I.A., **Hodgson, D.M.**, **Hubbard, S.M.**, **McArthur, A.D.**, **Poyatos-Moré, M.**, **Soutter, E.L.**, **Flint, S.S.** and **Matthews, W.** (2022) Deep-water Tectono-Stratigraphy at a Plate Boundary Constrained by Large N-Detrital Zircon and Micropaleontological Approaches: Peninsular Ranges Forearc, Baja California, Mexico. *Sediment. Rec.*, 1–15.

Kane, I.A., **McCaffrey, W.D.** and **Peakall, J.** (2010b) On the Origin of Paleocurrent Complexity Within Deep Marine Channel Levees. *J. Sediment. Res.*, **80**, 54–66.

Kilmer, F.H. (1963) Cretaceous and Cenozoic Stratigraphy and Paleontology, El Rosario area, Baja California, Mexico. University of California, Berkeley

Kim, B.C. and **Lowe, D.R.** (2004) Depositional processes of the gravelly debris flow deposits, South Dolomite alluvial fan, Owens Valley, California. *Geosci. J.*, **8**, 153–170.

Kimbrough, D.L., **Abbott, P.L.**, **Grove, M.**, **Smith, D.P.**, **Mahoney, J.B.**, **Moore, T.E.** and **Gehrels, G.E.** (2006) Contrasting cratonal provenances for Upper Cretaceous Valle Group quartzite clasts, Baja California. *Using Stratigr. Sedimentol. geochemistry to unravel Geol. Hist. Southwest. Cordillera*, 97–110.

Kimbrough, D.L., **Grove, M.** and **Morton, D.M.** (2015) Timing and significance of gabbro emplacement within two distinct plutonic domains of the Peninsular Ranges batholith, southern and Baja California. *Bull. Geol. Soc. Am.*, **127**, 19–37.

Kimbrough, D.L., **Smith, D.P.**, **Mahoney, J.B.**, **Moore, T.E.**, **Grove, M.**, **Gastil, R.G.**, **Ortega-Rivera, A.** and **Fanning, C.M.** (2001) Forearc-basin sedimentary response to rapid Late Cretaceous batholith emplacement in the Peninsular Ranges of southern and Baja California. *Geology*, **29**, 491–494.

Klaucke, I. and **Hesse, R.** (1996) Fluvial features in the deep-sea: new insights from the glacigenic submarine drainage system of the Northwest Atlantic Mid-Ocean Channel in the Labrador Sea. *Sediment. Geol.*, **106**, 223–234.

Knaust, D. (2019) The enigmatic trace fossil Tisoa Serres, 1840. *Earth-Science Rev.*, **188**, 123–147.

Kneller, B., **Bozetti, G.**, **Callow, R.**, **Dykstra, M.**, **Hansen, L.**, **Kane, I.**, **Li, P.**, **McArthur, A.**, **Catharina, A.S.**, **Dos Santos, T.** and **Thompson, P.** (2020) Architecture, process, and environmental diversity in a late Cretaceous slope channel system. *J. Sediment. Res.*, **90**, 1–26.

Kuenen, P.H. (1938) Density Currents in connection with the problem of Submarine Canyons. *Geol. Mag.*, **75**, 241–249.

Li, P., **Kneller, B.**, **Thompson, P.**, **Bozetti, G.** and **dos Santos, T.** (2018) Architectural and facies organisation of slope channel fills: Upper Cretaceous Rosario Formation, Baja California, Mexico. *Mar. Pet. Geol.*, **92**, 632–649.

Li, Y., **Pu, R.**, **Zhang, G.**, **Zhao, X.** and **Li, Y.** (2022) Architecture, controlling factors and evolution history of unidirectionally upstream-migrating turbidite channels: A case study from southern Qiongdongnan Basin, northern South China Sea. *Mar. Pet. Geol.*, **141**, 105706.

Lipman, P.W. (1992) Magmatism in the Cordilleran United States; Progress and problems. *Geol. North Am.*, **G-3**, 481–514.

Lo Iacono, C., **Guillén, J.**, **Guerrero, Q.**, **Durán, R.**, **Wardell, C.**, **Hall, R.A.**, **Aslam, T.**, **Carter, G.D.O.**, **Gales, J.A.** and **Huvenne, V.A.I.** (2020) Bidirectional bedform fields at the head of a submarine canyon (NE Atlantic). *Earth Planet. Sci. Lett.*, **542**, 116321.

Lowe, D.R. (1982) Sediment Gravity Flows: II Depositional Models with Special Reference to the Deposits of High-Density Turbidity Currents. *J. Sediment. Petrol.*, **52**, 279–297.

Maier, K.L., **Gales, J.A.**, **Paull, C.K.**, **Rosenberger, K.**, **Talling, P.J.**, **Simmons, S.M.**, **Gwiazda, R.**, **McGann, M.**, **Cartigny, M.J.B.**, **Lundsten, E.**, **Anderson, K.**, **Clare, M.A.**, **Xu, J.**, **Parsons, D.**, **Barry, J.P.**, **Wolfson-Schwehr, M.**, **Nieminski, N.M.** and **Sumner, E.J.** (2019) Linking direct measurements of turbidity currents to submarine canyon-floor deposits. *Front. Earth Sci.*, **7**, 1–18.

Maier, K.L., **Johnson, S.Y.** and **Hart, P.** (2018) Controls on submarine canyon head evolution: Monterey Canyon, offshore central California. *Mar. Geol.*, **404**, 24–40.

Martínez-Doñate, A., **Privat, A.M.-L.J.**, **Hodgson, D.M.**, **Jackson, C.A.L.**, **Kane, I.A.**, **Spychala, Y.T.**, **Duller, R.A.**, **Stevenson, C.**, **Keavney, E.**, **Schwarz, E.** and **Flint, S.S.** (2021) Substrate Entrainment, Depositional Relief, and Sediment Capture: Impact of a Submarine Landslide on Flow Process and Sediment Supply. *Front. Earth Sci.*, **9**, 1–23.

Matthews, W.A. and **Guest, B.** (2016) A Practical Approach for Collecting Large- n Detrital Zircon U-Pb Data sets by Quadrupole LA - ICP - MS. *Geostand. Geoanalytical Res.*, **41**, 161–180.

May, J.A. and **Warme, J.A.** (2007) An Ancient Submarine Canyon, Black's Beach, La Jolla, California, USA. In: *Atlas of deep-water outcrops: AAPG Studies in Geology 56* (Ed. T.H. Nilsen, R.D. Shew, G.S. Steffens, and J.R.J. Studlick), *The American Association of Petroleum Geologists*,

McArthur, A., **Kane, I.**, **Bozetti, G.**, **Hansen, L.** and **Kneller, B.C.** (2020) Supercritical flows overspilling from bypass-dominated submarine channels and the development of overbank bedforms. *Depos. Rec.*, **6**, 21–40.

McArthur, A.D. and **McCaffrey, W.D.** (2019) Sedimentary architecture of detached deep-marine canyons: Examples from the East Coast Basin of New Zealand. *Sedimentology*, **66**, 1067–1101.

Mcdowell, F.W., **Roldán-Quintana, J.** and **Connelly, J.N.** (2001) Duration of Late Cretaceous-early Tertiary magmatism in east-central Sonora, Mexico.

Micallef, A., **Mountjoy, J.J.**, **Barnes, P.M.**, **Canals, M.** and **Lastras, G.**

(2014) Geomorphic response of submarine canyons to tectonic activity: Insights from the Cook Strait canyon system, New Zealand. *Geosphere*, **10**, 905–929.

Millington, J.J. and **Clark, J.D.** (1995) The Charo/Arro Canyon-Mouth Sheet System, South-Central Pyrenees, Spain: A Structurally Influenced Zone of Sediment Dispersal. *J. Sediment. Res.*, **Vol. B65**, 443–454.

Morris, W. and **Busby-Spera, C.J.** (1990) A submarine-fan valley-levee complex in the Upper Cretaceous Rosario Formation: Implication for turbidite facies models. *Geol. Soc. Am. Bull.*, **102**, 900–914.

Morris, W.R. and **Busby, C.J.** (1996) The effects of tectonism on the high resolution sequence stratigraphic framework of non-marine to deep-marine deposits in the Peninsular Ranges forearc basin complex. In: *Field Conference Guide 1996. Pacific Section A.A.P.G.* (Ed. P.L. Abott and J.D. Cooper), *Pacific Section S.E.P.M.*, 381–408.

Mountjoy, J.J., **Barnes, P.M.** and **Pettinga, J.R.** (2009) Morphostructure and evolution of submarine canyons across an active margin: Cook Strait sector of the Hikurangi Margin, New Zealand. *Mar. Geol.*, **260**, 45–68.

Moxon, I.W. and **Graham, S.A.** (1987) History and controls of subsidence in the Late Cretaceous - Tertiary Great Valley forearc basin, California (USA). *Geology*, **15**, 626–629.

Nazarian, R.H., **Burns, C.M.**, **Legg, S.**, **Buijsman, M.C.**, **Kaur, H.** and **Arbic, B.K.** (2021) On the Magnitude of Canyon-Induced Mixing. *J. Geophys. Res. Ocean.*, **126**, 1–16.

Nemec, W. (1990) Aspects of Sediment Movement on Steep Delta Slopes. In: *Coarse-Grained Deltas*, *Blackwell Publishing Ltd.*, Oxford, UK, 29–73.

Normark, W.R. and **Piper, D.J.W.** (1991) Initiation Processes and Flow Evolution of Turbidity Currents: Implications for the Depositional Record. In: *From Shoreline to Abyss: Contributions in Marine Geology in Honor of Francis Parker Shepard* (Ed. R.H. Osborne), *SEPM Society for Sedimentary Geology*, 46, 207–230.

Palanques, A., **Masqué, P.**, **Puig, P.**, **Sanchez-Cabeza, J.A.**, **Frignani, M.** and **Alvisi, F.** (2008) Anthropogenic trace metals in the sedimentary record of the Llobregat continental shelf and adjacent Foix Submarine Canyon (northwestern Mediterranean). *Mar. Geol.*, **248**, 213–227.

Paull, C.K., **Talling, P.J.**, **Maier, K.L.**, **Parsons, D.**, **Xu, J.**, **Caress, D.W.**, **Gwiazda, R.**, **Lundsten, E.M.**, **Anderson, K.**, **Barry, J.P.**, **Chaffey, M.**, **O'Reilly, T.**, **Rosenberger, K.J.**, **Gales, J.A.**, **Kieft, B.**, **McGann, M.**, **Simmons, S.M.**, **McCann, M.**, **Sumner, E.J.**, **Clare, M.A.** and **Cartigny, M.J.** (2018) Powerful turbidity currents driven by dense basal layers. *Nat. Commun.*, **9**, 4114.

Pham, C.K., **Ramirez-Llodra, E.**, **Alt, C.H.S.**, **Amaro, T.**, **Bergmann, M.**, **Canals, M.**, **Company, J.B.**, **Davies, J.**, **Duineveld, G.**, **Galgani, F.**, **Howell, K.L.**, **Huvenne, V.A.I.**, **Isidro, E.**, **Jones, D.O.B.**, **Lastras, G.**, **Morato, T.**, **Gomes-Pereira, J.N.**, **Purser, A.**, **Stewart, H.**, **Tojeira, I.**, **Tubau, X.**, **Van Rooij, D.** and **Tyler, P.A.** (2014) Marine litter distribution and density in European seas, from the shelves to deep basins. PLoS One. doi: 10.1371/journal.pone.0095839

Pope, E.L., **Heijnen, M.S.**, **Talling, P.J.**, **Jacinto, R.S.**, **Gaillot, A.**, **Baker, M.L.**, **Hage, S.**, **Hasenhündl, M.**, **Heerema, C.J.**, **McGhee, C.**, **Ruffell,**

S.C., **Simmons, S.M.**, **Cartigny, M.J.B.**, **Clare, M.A.**, **Dennielou, B.**, **Parsons, D.R.**, **Peirce, C.** and **Urlaub, M.** (2022) Carbon and sediment fluxes inhibited in the submarine Congo Canyon by landslide-damming. Nat Geosci. doi: 10.1038/s41561-022-01017-x

Postma, G., **Nemec, W.** and **Kleinspehn, K.L.** (1988) Large floating clasts in turbidites: a mechanism for their emplacement. *Sediment. Geol.*, **58**, 47–61.

Puig, P., **Palanques, A.** and **Martín, J.** (2014) Contemporary Sediment-Transport Processes in Submarine Canyons. *Ann. Rev. Mar. Sci.*, **6**, 53–77.

Rasmussen, E.S. (1994) The relationship between submarine canyon fill and sea-level change: an example from Middle Miocene offshore Gabon, West Africa. *Sediment. Geol.*, **90**, 61–75.

Reading, H.G. (1980) Characteristics and Recognition of Strike-Slip Fault Systems. In: *Sedimentation in Oblique-Slip Mobile Zones* (Ed. P.F. Ballance and H.G. Reading), *The International Association of Sedimentologists*, 7–26.

Reading, H.G. (1996) Sedimentary environments: processes, facies, and stratigraphy, 3rd edn. *Blackwell Publishing*.

Rodgers, D.A. (1980) Analysis of Pull-Apart Basin Development Produced by En Echelon Strike-Slip Faults. In: *Sedimentation in Oblique-Slip Mobile Zones* (Ed. P.F. Ballance and H.G. Reading), *The International Association of Sedimentologists*, 27–41.

Schile, C.A. (1974) Sedimentology of the “El Gallo Formation” (Upper Cretaceous), El Rosario, Baja California, Mexico. San Diego State University

Schlacher, T., **Schlacher-Hoenlinger, M.**, **Williams, A.**, **Althaus, F.**, **Hooper, J.** and **Kloser, R.** (2007) Richness and distribution of sponge megabenthos in continental margin canyons off southeastern Australia. *Mar. Ecol. Prog. Ser.*, **340**, 73–88.

Sedlock, R.L. (2003) Geology and tectonics of the Baja California peninsula and adjacent areas. 1–42 pp.

Seidler, L. (2000) Incised submarine canyons governing new evidence of Early Triassic rifting in East Greenland. **161**, 267–293.

Sharman, G.R., **Sharman, J.P.** and **Sylvester, Z.** (2018) detritalPy: A Python-based toolset for visualizing and analysing detrital geo-thermochronologic data. *Depos. Rec.*, **4**, 202–215.

Shepard, F.P. (1972) Submarine canyons. *Earth-Science Rev.*, **8**, 1–12.

Slootman, A. and **Cartigny, M.J.B.** (2020) Cyclic steps: Review and aggradation-based classification. *Earth-Science Rev.*, **201**, 102949.

Smith, D.P., **Kvitek, R.**, **Iampietro, P.J.** and **Wong, K.** (2007) Twenty-nine months of geomorphic change in upper Monterey Canyon (2002–2005). *Mar. Geol.*, **236**, 79–94.

Sohn, Y.K. (2000) Depositional Processes of Submarine Debris Flows in the Miocene Fan Deltas, Pohang Basin, SE Korea with Special Reference to Flow Transformation. SEPM J Sediment Res. doi: 10.1306/D4268C3E-2B26-11D7-8648000102C1865D

Stevenson, C.J., **Jackson, C.A.-L.**, **Hodgson, D.M.**, **Hubbard, S.M.** and **Eggenhuisen, J.T.** (2015) Deep-Water Sediment Bypass. *J. Sediment. Res.*, **85**, 1058–1081.

Su, M., **Lin, Z.**, **Wang, C.**, **Kuang, Z.**, **Liang, J.**, **Chen, H.**, **Liu, S.**, **Zhang, B.**, **Luo, K.**, **Huang, S.** and **Wu, Q.** (2020) Geomorphologic and infilling characteristics of the slope-confined submarine canyons in the Pearl River Mouth Basin, northern South China Sea. *Mar. Geol.*, **424**, 106166.

Symons, W.O., **Sumner, E.J.**, **Paull, C.K.**, **Cartigny, M.J.B.**, **Xu, J.P.**, **Maier, K.L.**, **Lorenson, T.D.** and **Talling, P.J.** (2017) A new model for turbidity current behavior based on integration of flow monitoring and precision coring in a submarine canyon. *Geology*, **45**, 367–370.

Talling, P.J., **Cartigny, M.J.B.**, **Pope, E.**, **Baker, M.**, **Clare, M.A.**, **Heijnen, M.**, **Hage, S.**, **Parsons, D.R.**, **Simmons, S.M.**, **Paull, C.K.**, **Gwiazda, R.**, **Lintern, G.**, **Hughes Clarke, J.E.**, **Xu, J.**, **Silva Jacinto, R.** and **Maier, K.L.** (2023) Detailed monitoring reveals the nature of submarine turbidity currents. Nat Rev Earth Environ. doi: 10.1038/s43017-023-00458-1

Taviani, M., **Foglini, F.**, **Castellan, G.**, **Montagna, P.**, **McCulloch, M.T.** and **Trotter, J.A.** (2023) First assessment of anthropogenic impacts in submarine canyon systems off southwestern Australia. *Sci. Total Environ.*, **857**, 159243.

Tek, D.E., **McArthur, A.D.**, **Poyatos-Moré, M.**, **Colombera, L.**, **Patacci, M.**, **Craven, B.** and **McCaffrey, W.D.** (2021) Relating seafloor geomorphology to subsurface architecture: How mass-transport deposits and knickpoint-zones build the stratigraphy of the deep-water Hikurangi Channel. *Sedimentology*, **68**, 3141–3190.

Tian, H., **Lin, C.**, **Zhang, Z.**, **Li, H.**, **Zhang, B.**, **Zhang, M.**, **Liu, H.** and **Jiang, J.** (2021) Depositional architecture, evolution and controlling factors of the Miocene submarine canyon system in the Pearl River Mouth Basin, northern South China Sea. *Mar. Pet. Geol.*, 104990.

Tsuji, T., **Ashi, J.** and **Ikeda, Y.** (2014) Strike-slip motion of a mega-splay fault system in the Nankai oblique subduction zone. *Earth, Planets Sp.*, **66**, 120.

Vetter, E.W., **Smith, C.R.** and **De Leo, F.C.** (2010) Hawaiian hotspots: enhanced megafaunal abundance and diversity in submarine canyons on the oceanic islands of Hawaii. *Mar. Ecol.*, **31**, 183–199.

Von der Borch, C.C., **GRADY, A.E.**, **ALDAM, R.**, **MILLER, D.**, **NEUMANN, R.**, **ROVIRA, A.** and **EICKHOFF, K.** (1985) A large-scale meandering submarine canyon: outcrop example from the late Proterozoic Adelaide Geosyncline, South Australia. *Sedimentology*, **32**, 507–518.

Walker, R.G. (1975) Generalized facies models for resedimented conglomerates of turbidite association. *Bull. Geol. Soc. Am.*, **86**, 737–748.

Wetmore, P.H., **Hughes, S.S.**, **Stremtan, C.**, **Ducea, M.N.** and **Alsleben, H.** (2014) Tectonic implications of postcontractional magmatism of the Alisitos arc segment of the Peninsular Ranges, Baja California, Mexico. *Mem. Geol. Soc. Am.*, **211**, 669–690.

Wetmore, P.H., **Schmidt, K.L.**, **Paterson, S.R.** and **Herzig, C.** (2002) Tectonic implications for the along-strike variation of the Peninsular Ranges batholith, southern and Baja California. *Geology*, **30**, 247–250.

Wood, G.D., **Gabriel, A.M.** and **Lawson, J.C.** (1996) Palynological techniques – processing and microscopy. In: *Palynology: principles and applications* (Ed. J. Jansonius and D.C. MaxGregor), 29–50.

Wu, J.E., **McClay, K.**, **Whitehouse, P.** and **Dooley, T.** (2009) 4D analogue modelling of transtensional pull-apart basins. *Mar. Pet. Geol.*, **26**, 1608–1623.

Wu, N., **Nugraha, H.D.**, **Zhong, G.** and **Steventon, M.J.** (2022) The role of mass-transport complexes in the initiation and evolution of submarine canyons. *Sedimentology*, **69**, 2181–2202.

Xu, J.P. and **Noble, M.A.** (2009) Currents in Monterey Submarine Canyon. *J. Geophys. Res.*, **114**, C03004.

Zhu, M., **Graham, S.**, **Pang, X.** and **McHargue, T.** (2010) Characteristics of migrating submarine canyons from the middle Miocene to present: Implications for paleoceanographic circulation, northern South China Sea. *Mar. Pet. Geol.*, **27**, 307–319.

Figure, captions, and table references:

1. (Gastil *et al.*, 1971; Kane *et al.*, 2022)
2. (Busby *et al.*, 1998; Tsuji *et al.*, 2014)
3. –
4. –
5. –
6. –
7. –
8. –
9. –
10. –
11. –
12. –
13. –
14. –
15. –
16. –
17. -
18. (Balster-Gee *et al.*, 2018; Maier *et al.*, 2018)

Table 1: (Walker, 1975; Lowe, 1982; Postma *et al.*, 1988; Nemec, 1990; Cronin, 2018; Boulesteix *et al.*, 2019; Slootman & Cartigny, 2020)

Figures

This document's dimensions are set to the dimensions of Sedimentology pages and figure dimensions:

Full Page:

170 mm width	230 mm height

Figure widths:

80 mm	1 column
112 mm	2/3 page
170 mm	Full page width

Fig.	Width
1	2/3 page
2	1 column
3	Full page width
4	Full page width
5	Full page width (2 pages)
6	Full page width
7	Full page width
8	Full page width
9	Full page width
10	Full page width
11	Full page width - Landscape
12	Full page width
13	Full page width
14	Full page width
15	Full page width
16	Full page width
17	Full page width
18	Full page width

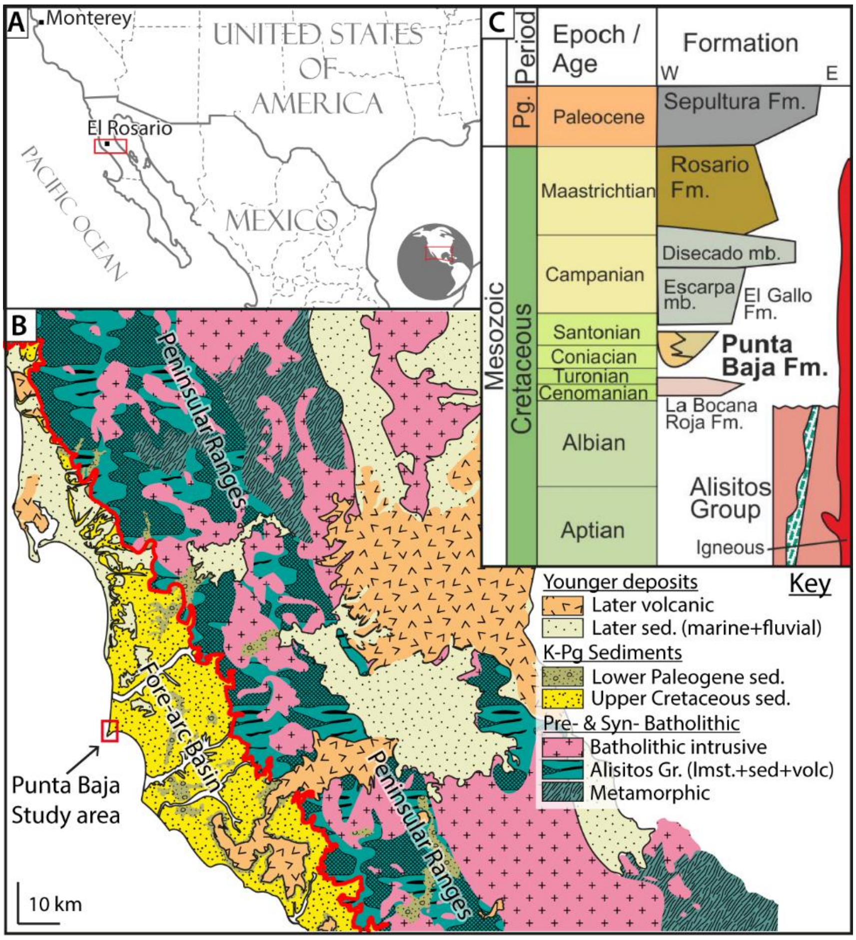

Figure 1: **A)** Location of the study area on the Baja California peninsula, Mexico. **B)** Geological map of the Baja California peninsula (simplified from Gastil *et al.* (1971)). Lithologies grouped for the purposes of this study in: pre- & syn-batholitic rocks of the Peninsular Ranges (blue and pink) that are the bedrock and source of the studied Late Cretaceous sedimentary systems (yellow), and younger deposits (pale yellow and orange). Note that modern sediment conduits (white) drain straight from the Peninsular Ranges into the Pacific Ocean, probably in a similar way to sedimentary systems since the Cretaceous. **C)** Upper Cretaceous and Palaeocene stratigraphy of the study area with the duration of magmatism on the peninsula highlighted (Kane *et al.*, 2022), the Punta Baja Fm. canyon fill in bold.

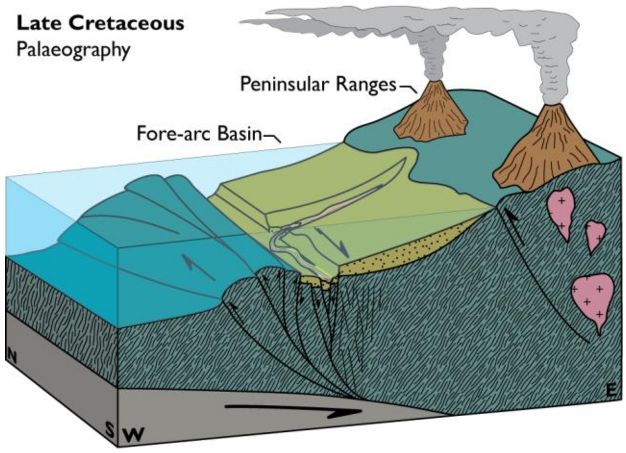

Figure 2: Schematic paleogeography during the Late Cretaceous continental arc phase (Modified from Busby *et al.* (1998) and Tsuji *et al.* (2014)) showing the active magmatism and uplift in the Peninsular Ranges, with steep and short sedimentary systems draining and depositing westwards into the Pacific Ocean-facing fore-arc basin, steered by complex structural topography. Colours correspond to Figure 1b.

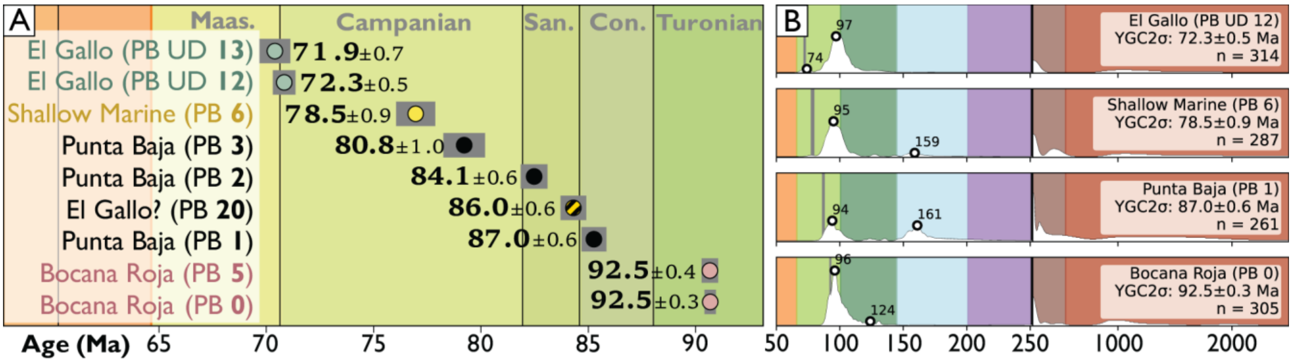

Figure 3: A) *Large-N Detrital Zircon ages of samples collected from the bedrock Bocana Roja Formation, Punta Baja Formation submarine canyon fill, and shallow marine to fluvial El Gallo Formation.* ***B)*** *Detrital Zircon age distributions for representative samples with statistically most relevant populations, yielding a Maximum Depositional Age (MDA) using the YGC 2σ methodology* (Dickinson and Gehrels 2009). *Note the change in timescale increments around 250 Ma (Palaeozoic-Mesozoic)*

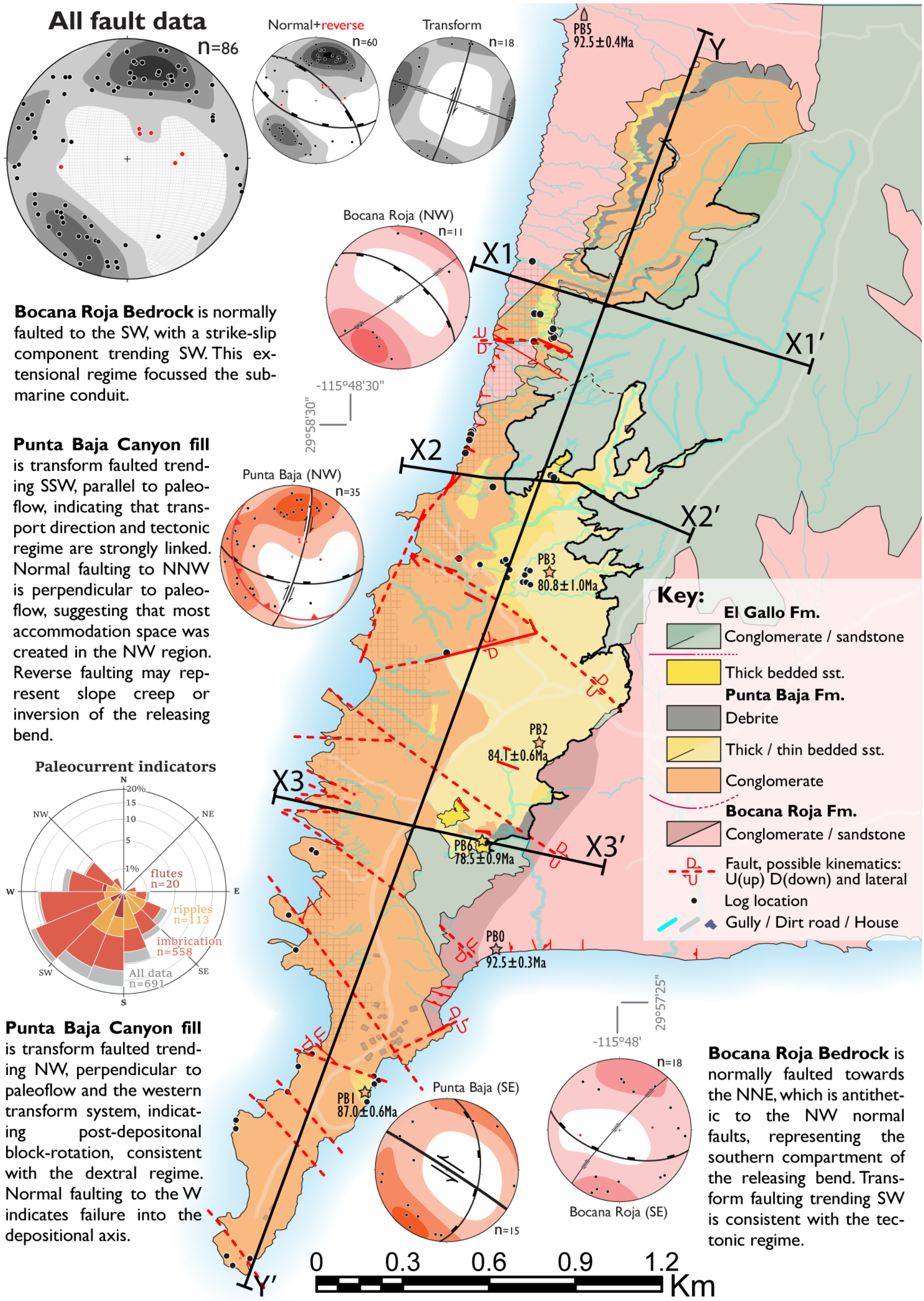

Figure 4: Formation and facies map of the field area with major fault traces, location of cross sections, and equal-area rose diagram of palaeo-current indicators. Fault plane orientations plotted as poles and grouped per formation and location. Fault kinematics on traces on the map are displayed with vertical and lateral components that could both explain the outcrop pattern, however the exact kinematics are unknown.

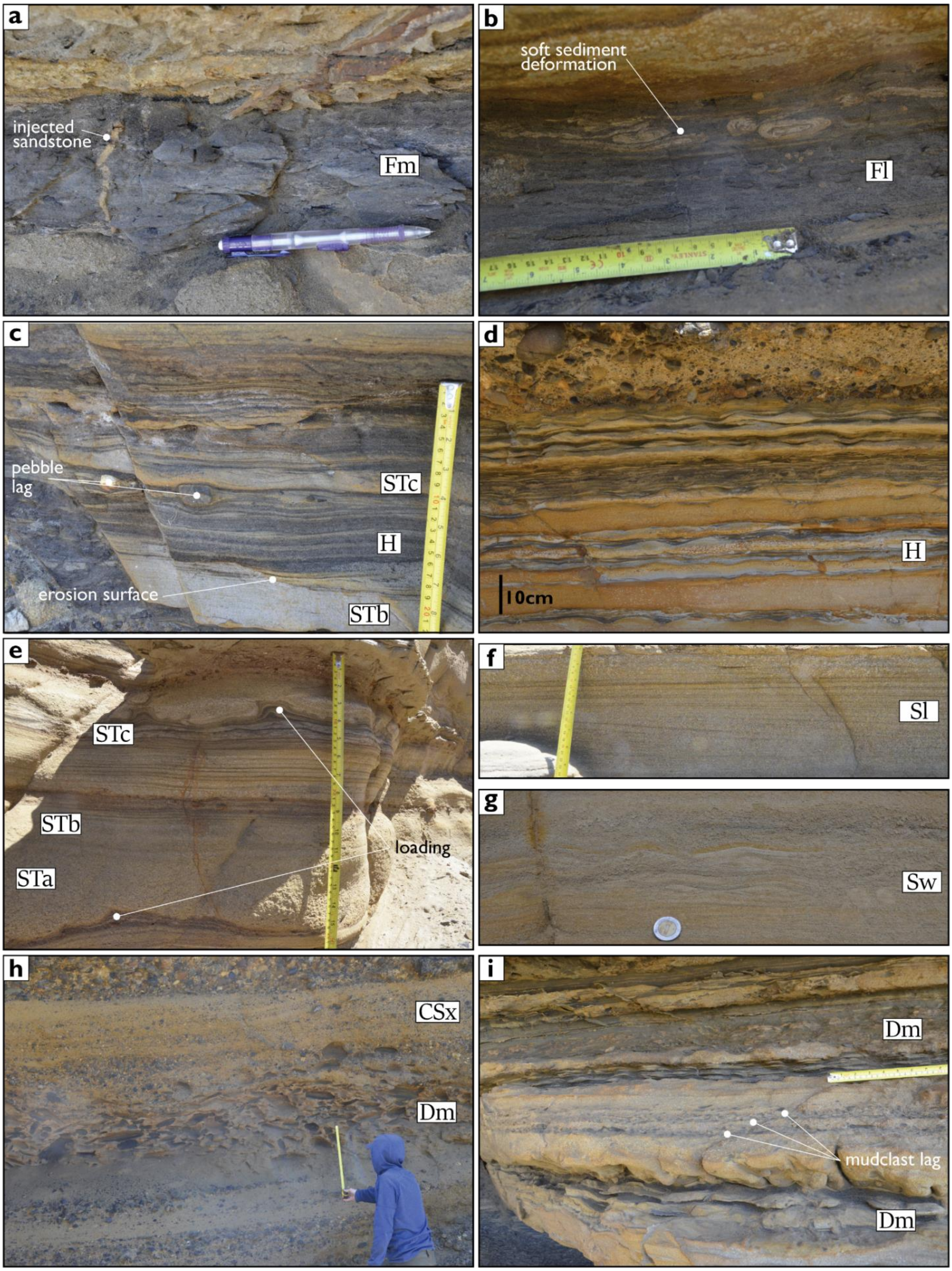

***Figure 5:** Representative facies field photographs of facies in **Error! Reference source not found.**.*

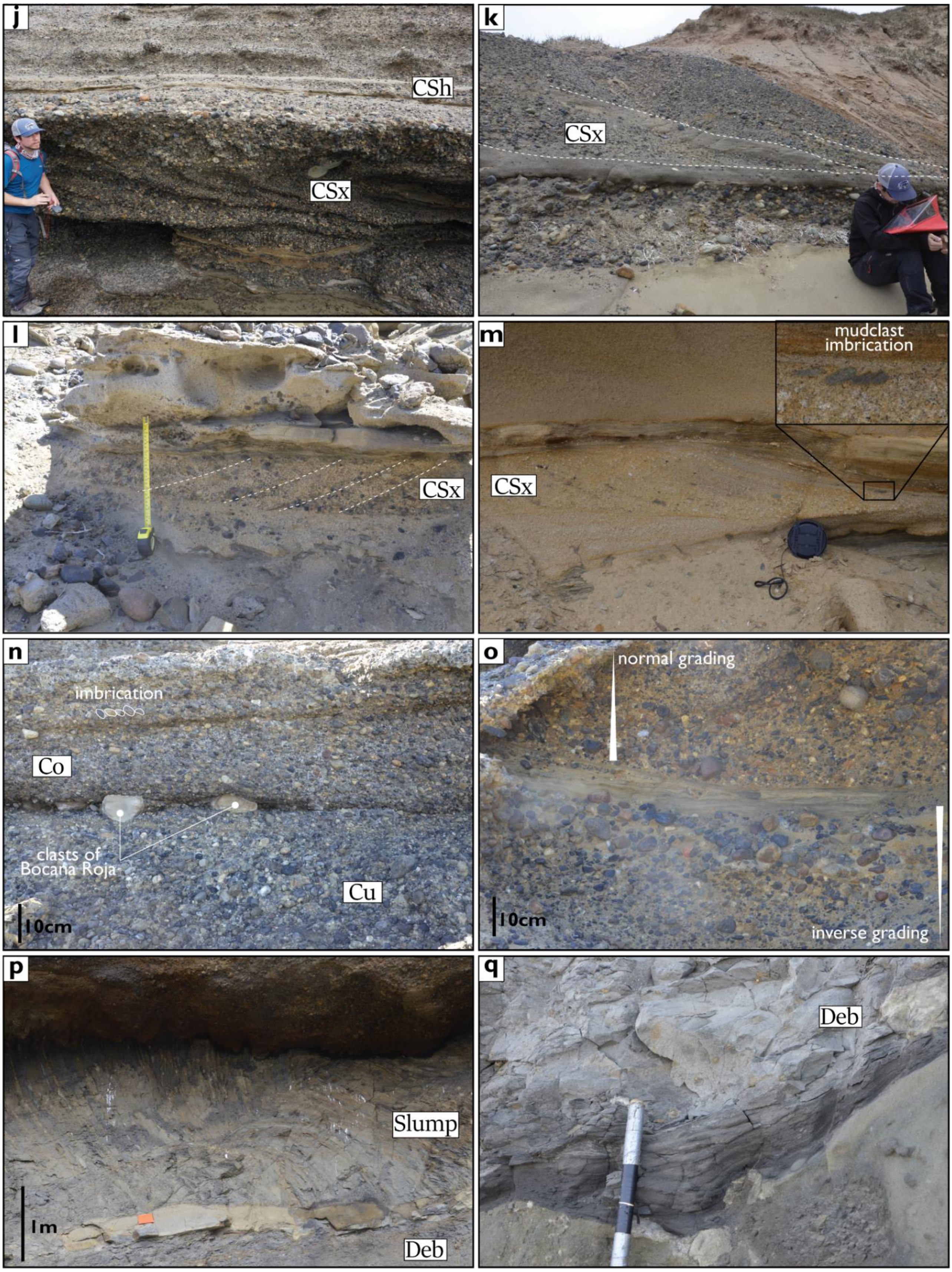

Figure 5 (continued)

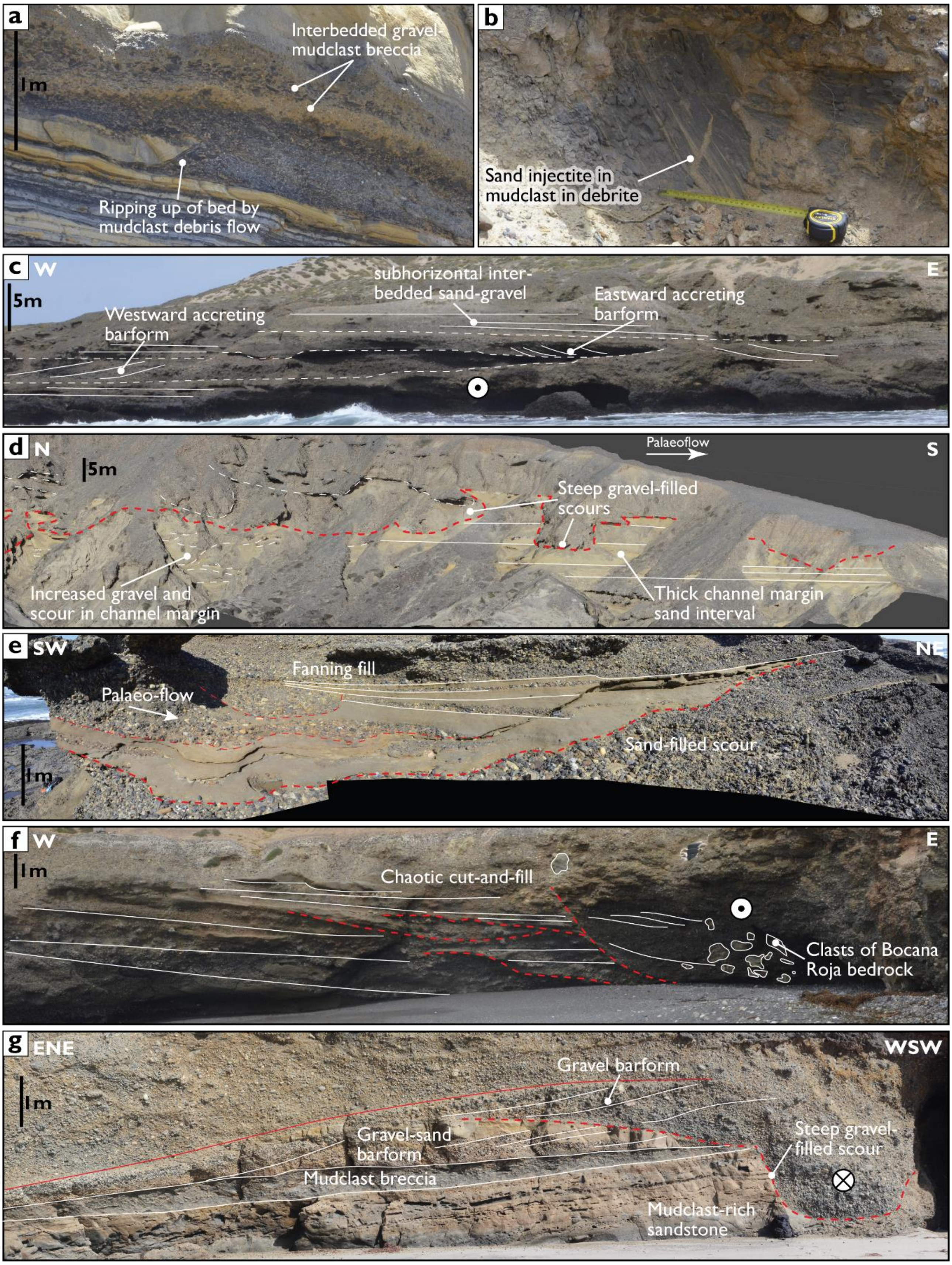

Figure 6: *Field photographs representing depositional and erosional bedforms in coarse-grained deposits.*

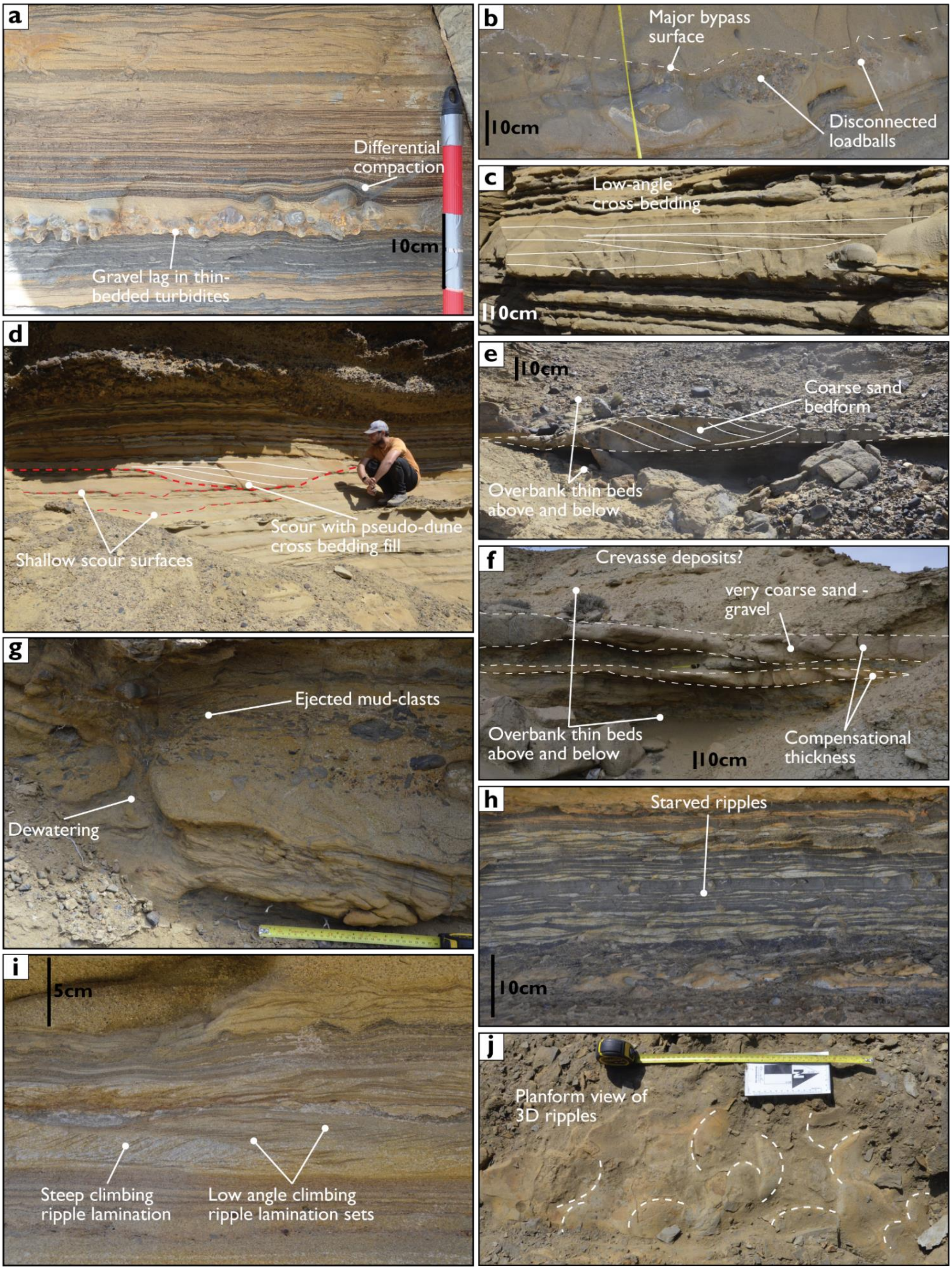

Figure 7: *Field photographs representing depositional and erosional bedforms in generally fine-grained deposits.*

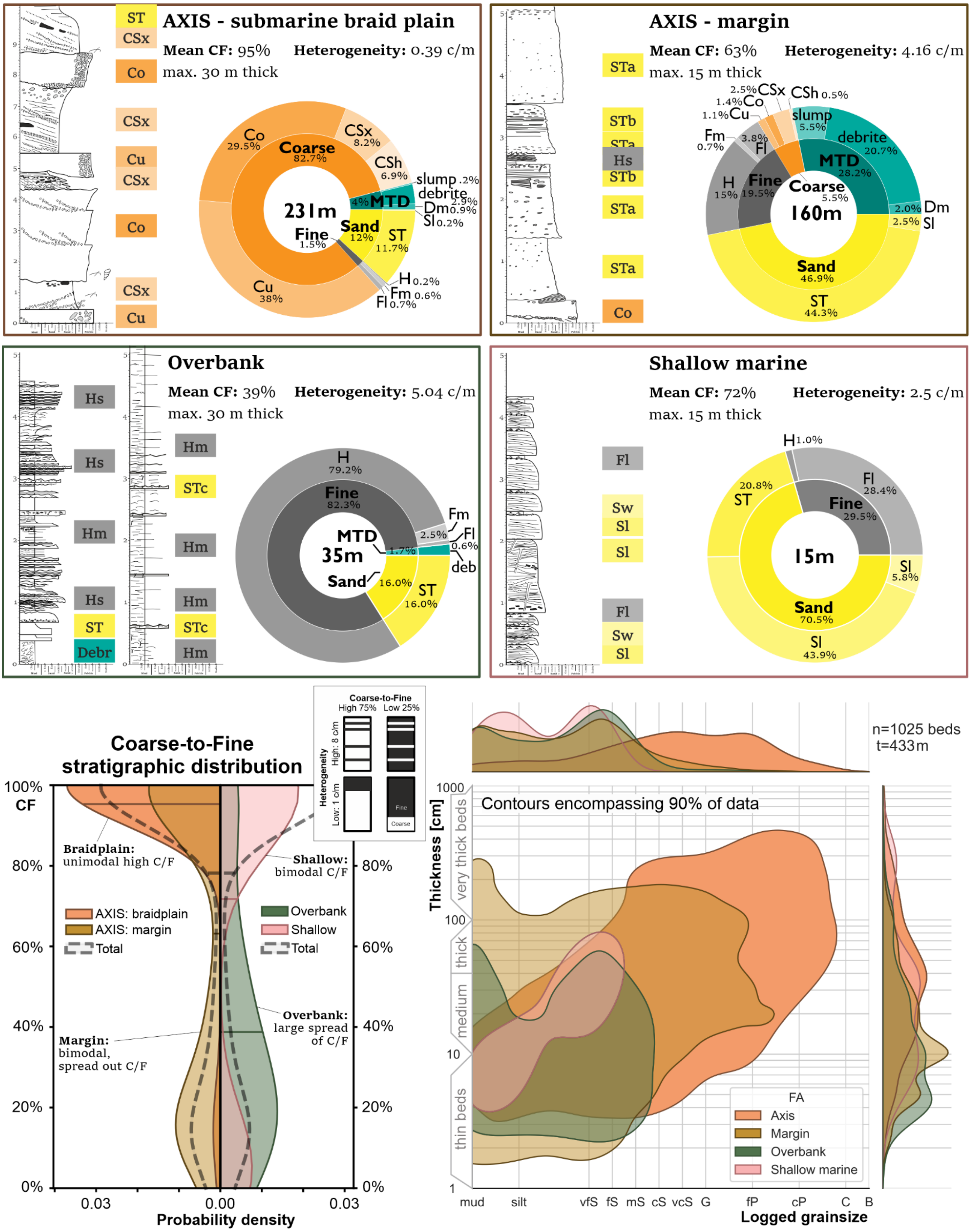

*Figure 8: Overview, characteristics, and statistics of facies associations. Representative measured sections of each facies association are labelled with facies (**Error! Reference source not found.**). Donut plots of facies make-up in percentage of total stratigraphic thickness per facies association, categorised by mean grainsize being in the mud, sand, or coarser range. Mean CF represents the percentage of stratigraphy with a logged grainsize coarser than silt. Heterogeneity (in changes per meter or c/m) indicates how the coarse vs. fine lithologies are distributed; high heterogeneity means that coarse and fine lithologies are interspersed, while low heterogeneity implies a more clustered distribution and thicker intervals of the same class. Logged grainsize versus bed thickness of beds in each facies association. Coarse-to-Fine distribution per bed per facies association, on a probability density scale, which gives more detail than the mean value.*

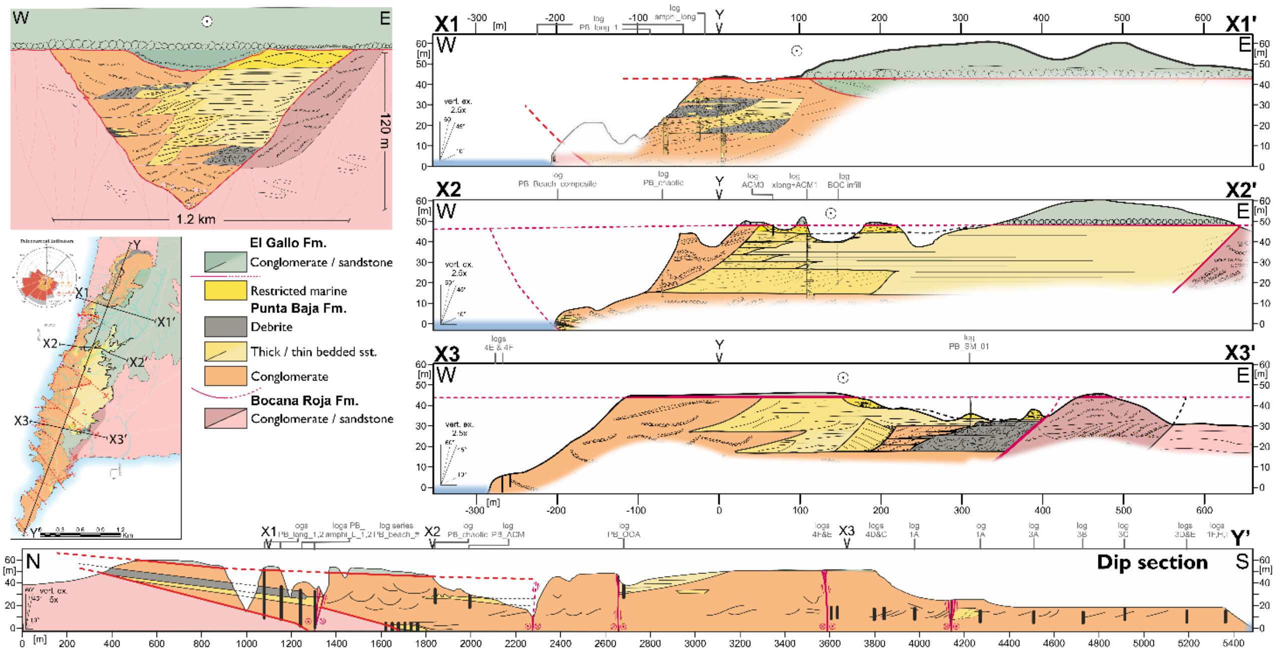

Figure 9: *Strike and dip panels with projected mapped facies boundaries, logged sections, and UAV-assisted orientation of surfaces. Note vertical exaggeration in each panel. Due to regional tectonic deformation, the strike-oriented panels provide different windows into the stratigraphic order; panel X3 covers the lowest stratigraphy, panel X1 the highest stratigraphy of the exposed canyon fill.*

Figure 10 *(next page): Field photographs and 3D-model renders of the variable nature of the canyon fill erosional contact with the underlying Bocana Roja Formation. a) Steep dune-scale cross-bedded conglomerates representing alluvial braided stream deposits of the Bocana Roja Formation on the eastern side of the canyon fill erosion surface. b) Finer-grained floodplain deposits of the Bocana Roja Formation to the west and further east of the canyon fill erosion surface (see lense cap for scale). c) Western canyon wall contact between Bocana Roja Formation floodplain deposits and Punta Baja submarine canyon fill conglomerates. d) Western canyon wall scalloped contact between Bocana Roja floodplain deposits and Punta Baja submarine thin-bedded turbidites and dark mud pebbly debrites, representing a chute or gully on the canyon wall and inferring major bypass. e) Western canyon wall contact between Bocana Roja Formation floodplain deposits and a variety of Punta Baja Fomration submarine facies (more detail in* ***Figure 116****). f) Eastern canyon wall contact between Bocana Roja Formation floodplain deposits and onlapping Punta Baja Formation submarine canyon fill thin-bedded overbank turbidites.*

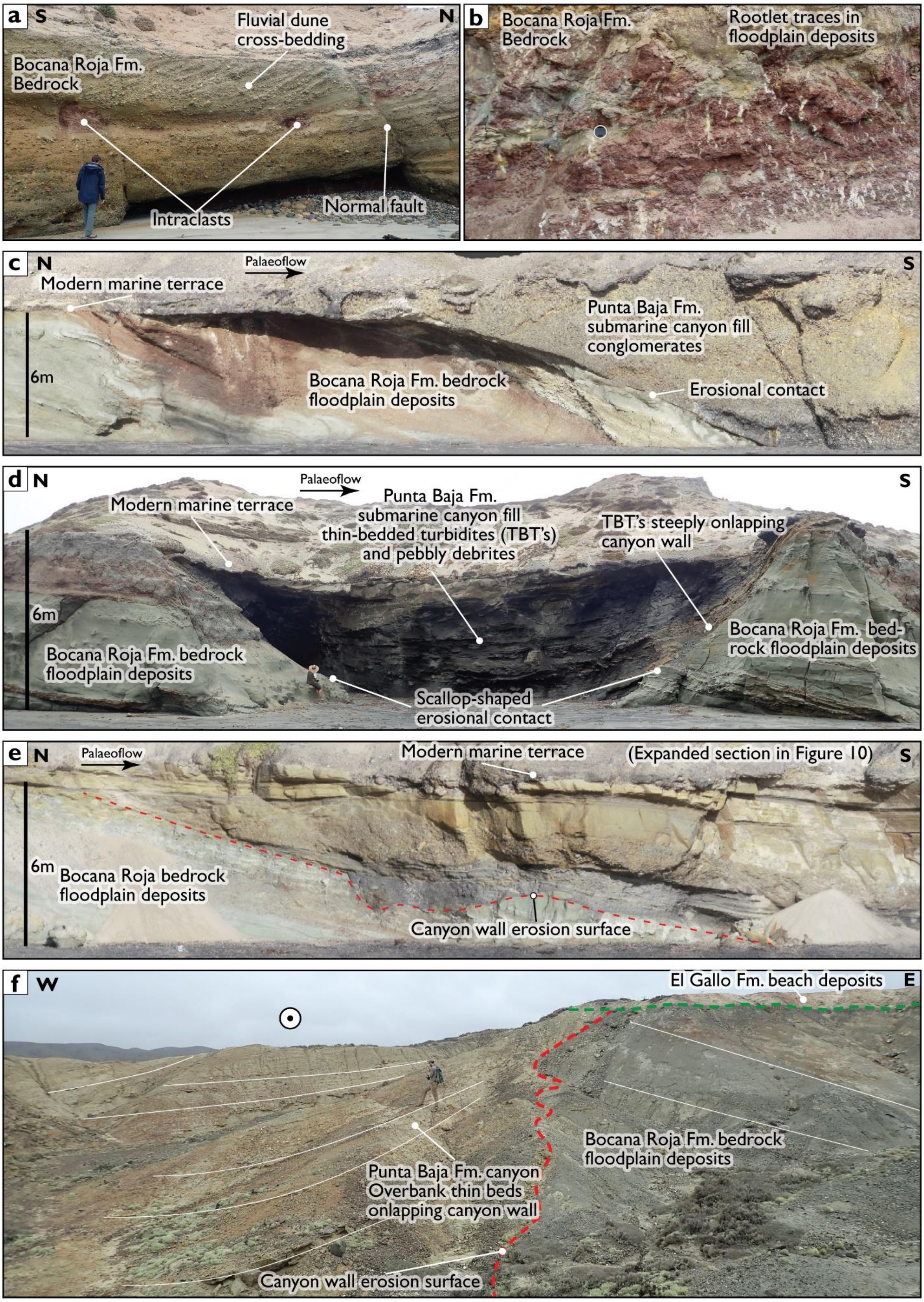
a
S
N
Fluvial dune cross-bedding
Bocana Roja Fm. Bedrock
Intraclasts
Normal fault
b
Bocana Roja Fm. Bedrock
Rootlet traces in floodplain deposits
c
N
Palaeoflow
S
Modern marine terrace
Punta Baja Fm. submarine canyon fill conglomerates
6m
Bocana Roja Fm. bedrock floodplain deposits
Erosional contact
d
N
Palaeoflow
S
Punta Baja Fm. submarine canyon fill thin-bedded turbidites (TBT's) and pebbly debrites
Modern marine terrace
TBT's steeply onlapping canyon wall
6m
Bocana Roja Fm. bed-rock floodplain deposits
Bocana Roja Fm. bedrock floodplain deposits
Scallop-shaped erosional contact
e
N
Palaeoflow
Modern marine terrace
(Expanded section in Figure 10)
S
6m
Bocana Roja bedrock floodplain deposits
Canyon wall erosion surface
f
W
El Gallo Fm. beach deposits
E
Bocana Roja Fm. bedrock floodplain deposits
Punta Baja Fm. canyon Overbank thin beds onlapping canyon wall
Canyon wall erosion surface

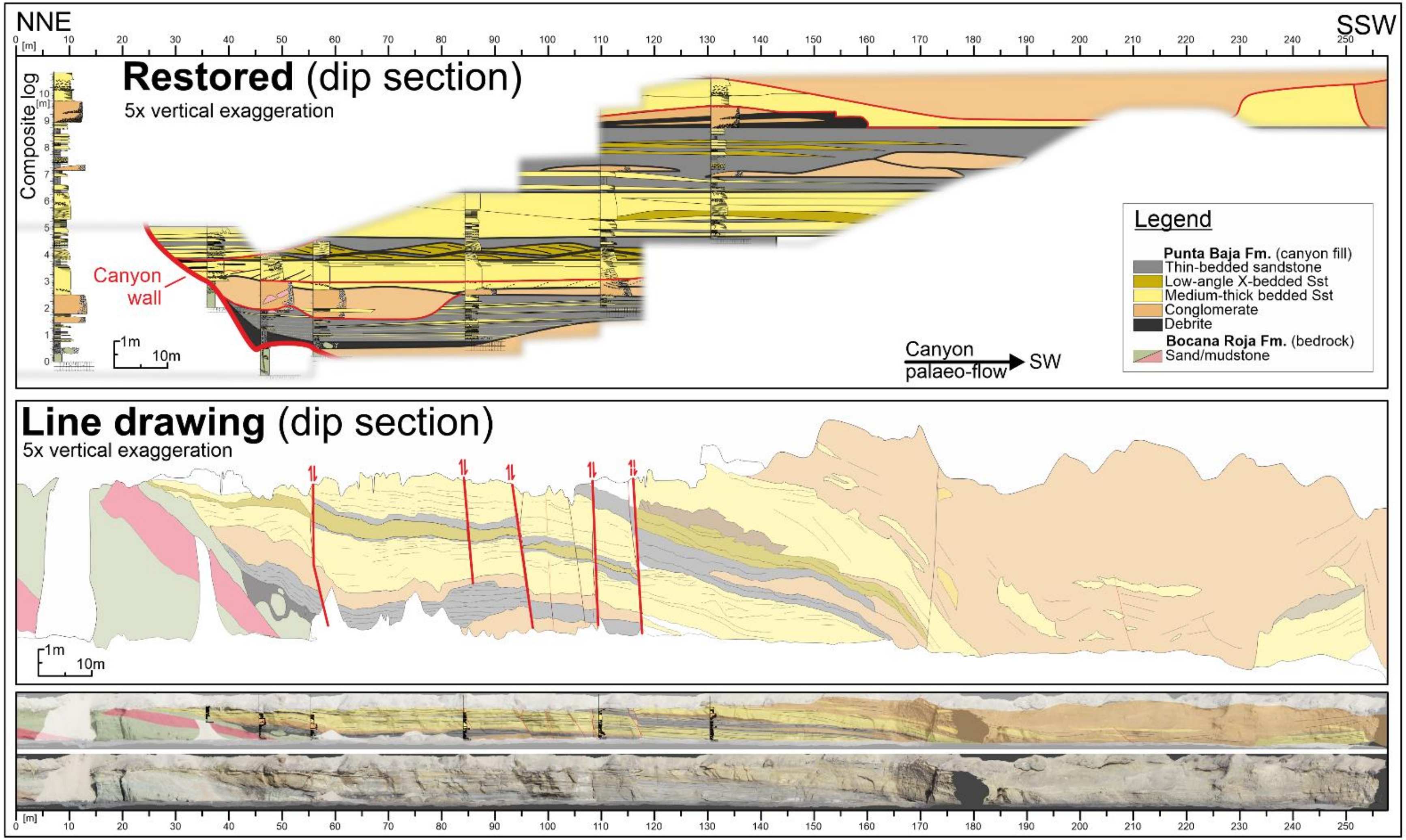

Figure 116: *Canyon wall onlap styles*

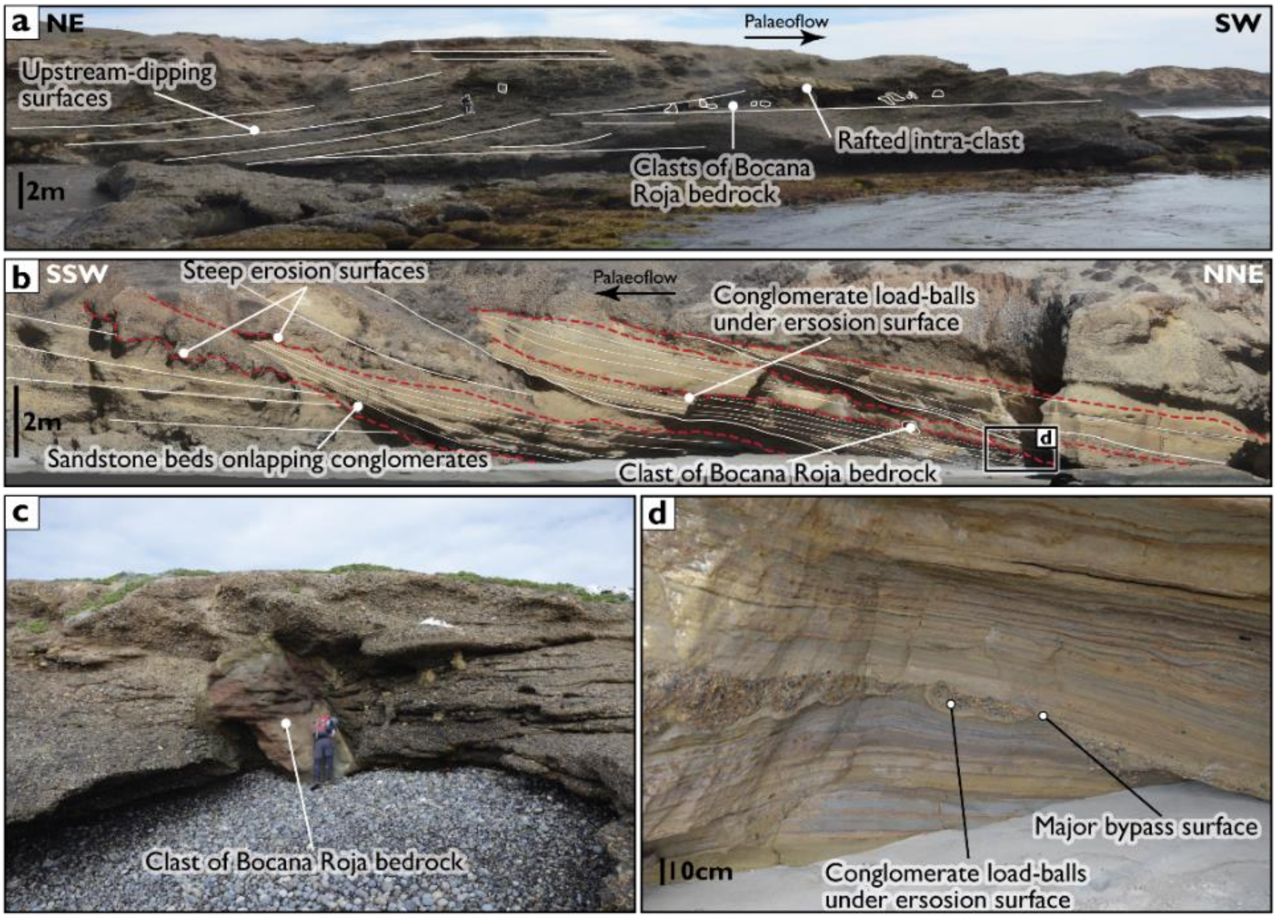

Figure 7: Characteristics of the lower canyon fill. a) Amalgamated conglomeratic deposits with clasts of Bocana Roja bedrock and a rafted intraformational clast, showing common up-stream dipping surfaces; b) Steep erosion surfaces overlain by conglomerate and onlapped by medium to thin-bedded turbidites. Erosion surfaces stepping up-stream, possibly representing migrating channels on the submarine braid plain, filled with sand-rich turbidites; c) a large clast (4 m diameter) of Bocana Roja bedrock with original bedding preserved, within Punta Baja canyon fill conglomerates; d) Detail of b showing conglomerate load-balls within thin-bedded turbidites, sometimes completely removed and the only evidence of high-energy deposits that were since removed, and thus representing a major bypass surface.

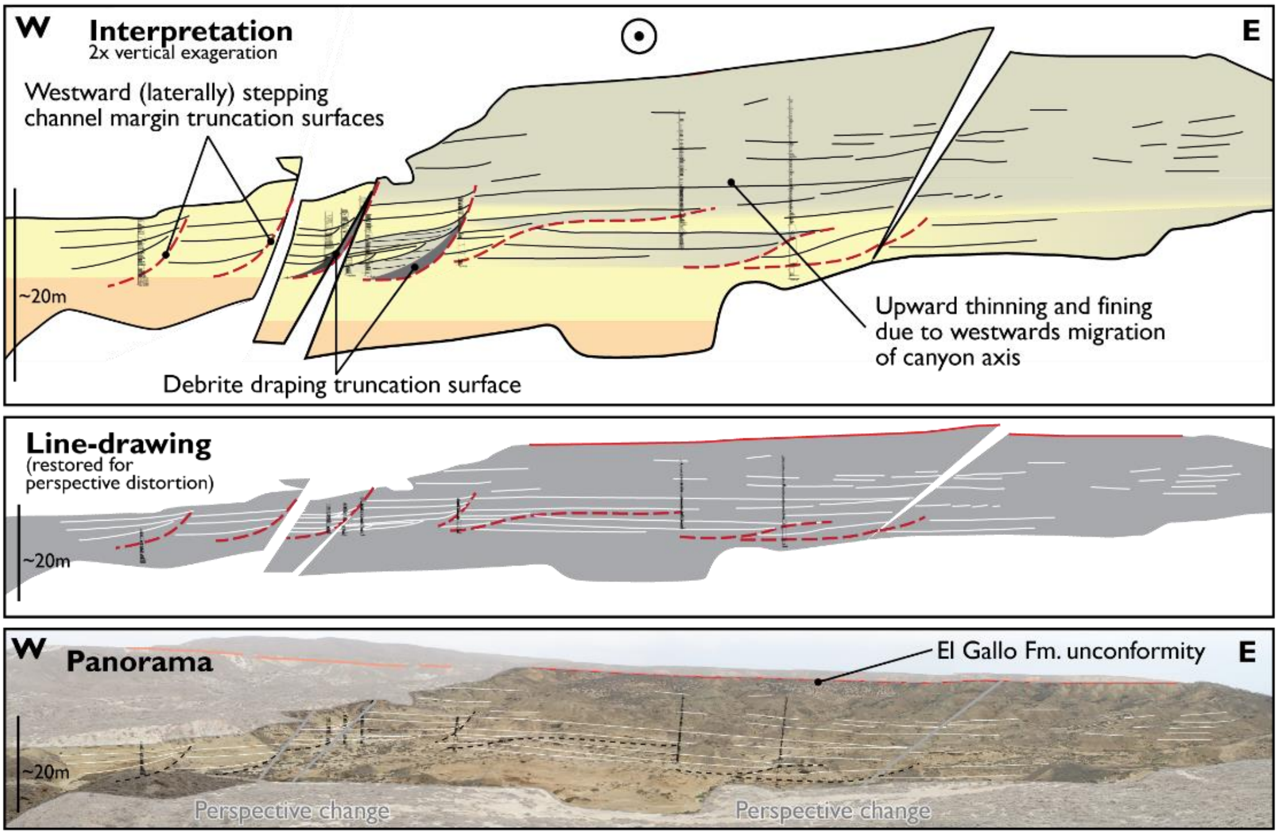

Figure 13: *Photo panel and reconstructed interpretation of westward laterally stepping channel margin deposits. The vertical fining facies succession and westward stepping of erosion surfaces reflect a westward migration of the canyon axis, resulting in decreasing energy levels in its eastern parts. Multiple erosion surfaces are overlain by muddy debrites, reflecting the bank failure and erosion upstream of this location.*

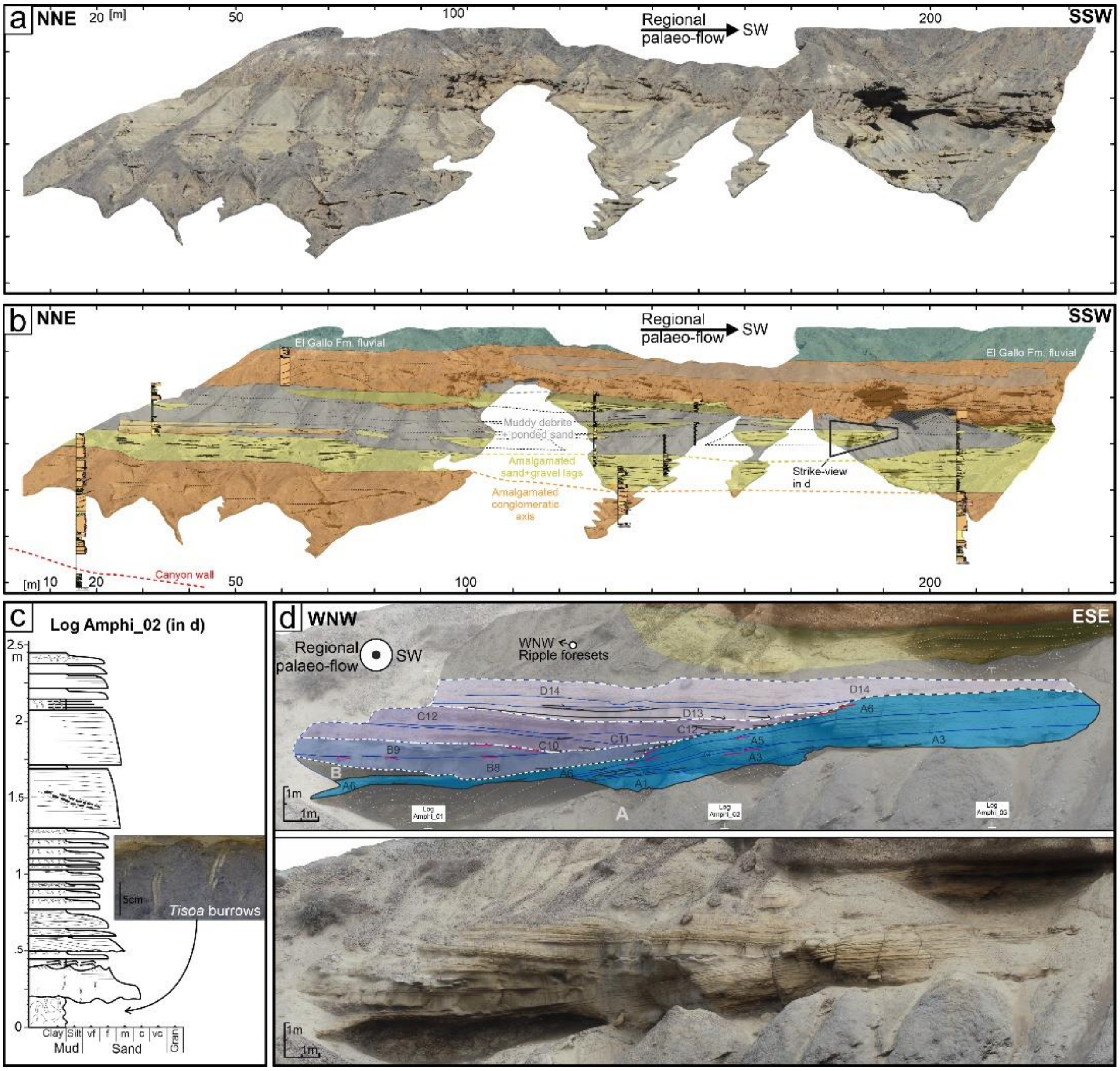

Figure 14: a) 3D outcrop model orthographic render of northern cliff dip-section; **b)** Interpretation highlighting depositional environments, and measured sections; **c)** Example sedimentary log through a ponded sandstone body within the mass transport complex. The *Tisoa* burrows suggest that the erosion surfaces were sustained open sediment conduits before filling. **d)** Strike view of a sandstone body within the MTC, interpreted as several phases of sand deposition over a partly mobile substrate, causing complex dip orientations and cross-cutting relationships.

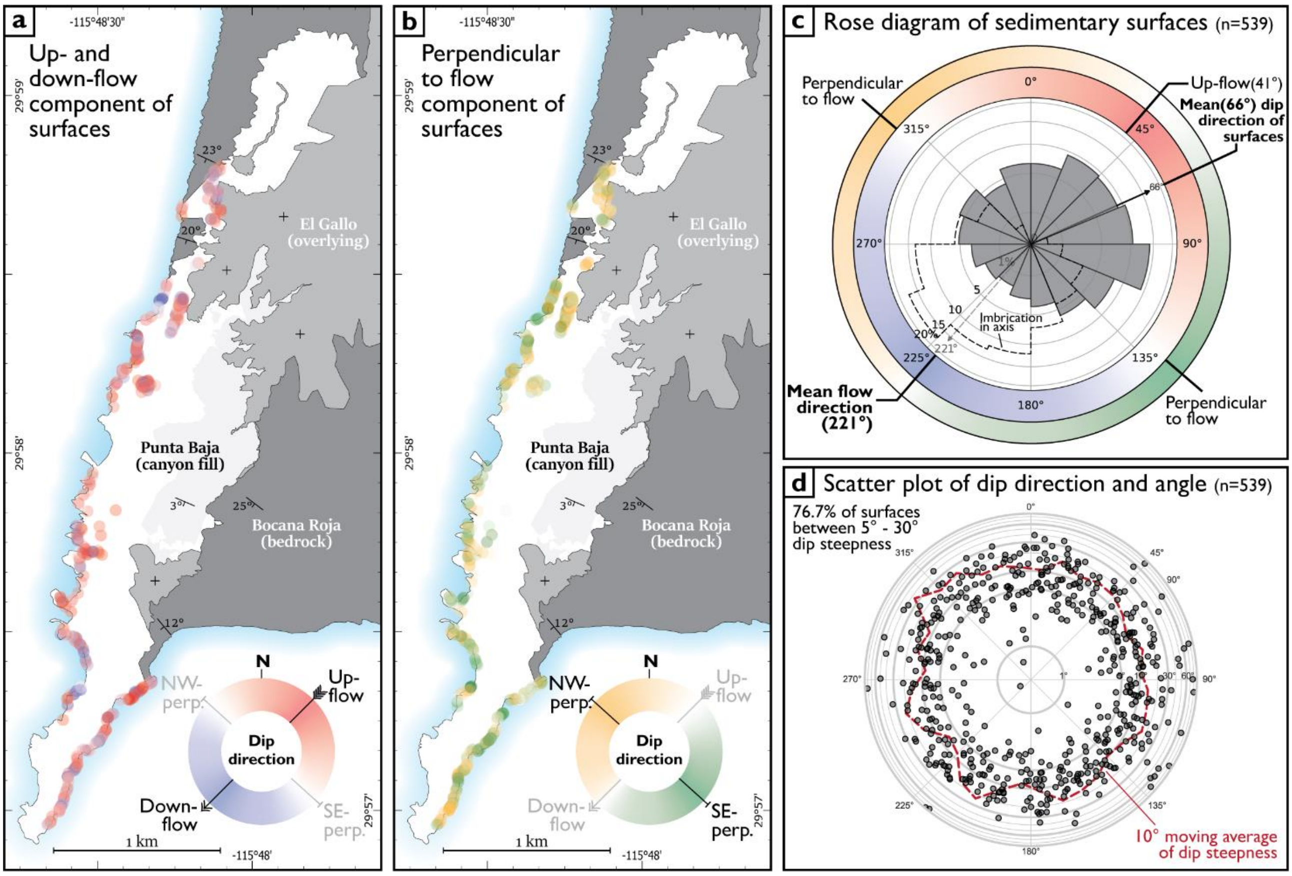

__Figure 15:__ Orientation and spatial distribution of 539 virtual 3D outcrop model measured sedimentary surfaces in the Punta Baja conglomeratic canyon fill, compared to the mean sediment transport direction in axial conglomerate deposits. __a)__ Location of interpreted surfaces, coloured by dip direction relative to mean palaeoflow direction, focussing on up- and down-stream trends (see c for colour legend). Up-stream dipping surfaces dominate most locations, even with the canyon fill tectonic tilt dipping 3° downstream; __b)__ Location of the same interpreted surfaces, coloured by dip direction relative to mean palaeoflow direction, focussing on palaeoflow-perpendicular trends (see c for colour legend). Eastwards and westwards dipping surfaces occur evenly dispersed, suggesting no preferred orientation of flow-perpendicular surfaces; __c)__ Rose diagram comparing mean conglomerate imbrication transport direction (dashed, SW 221° mean) to dip direction of sedimentary surfaces (grey, ENE 066° mean), showing a clear antithetic relation; __d)__ Scatter plot of dip direction and dip angle (note logarithmic radial axis) of sedimentary surfaces. More than 75% of sedimentary surfaces dip 5 – 30°, with no clear relation between dip direction and steepness, confirming that only the number of preserved surfaces dipping upstream is greater than downstream, and not the surface steepness.

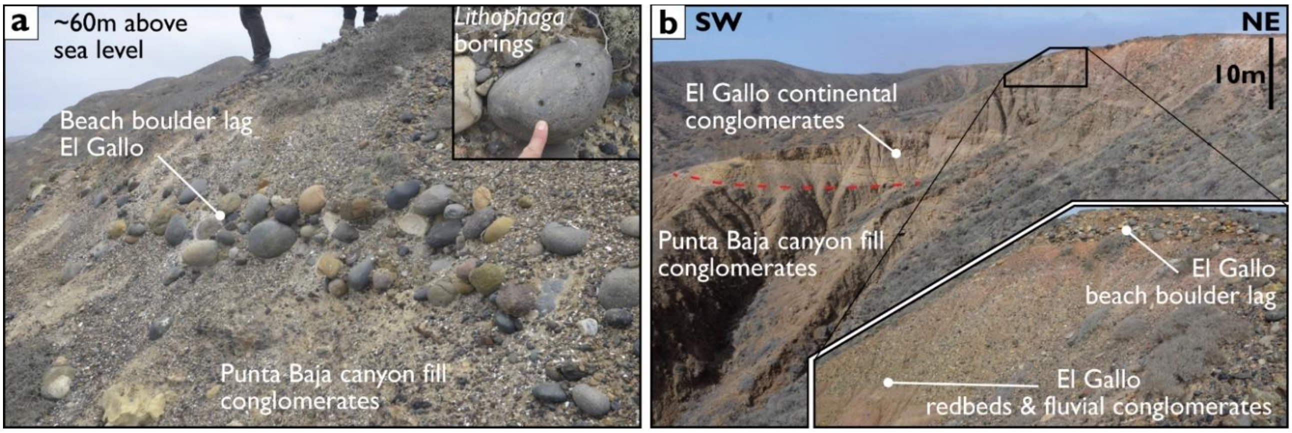

Figure 16: *Expression of the El Gallo unconformity.*

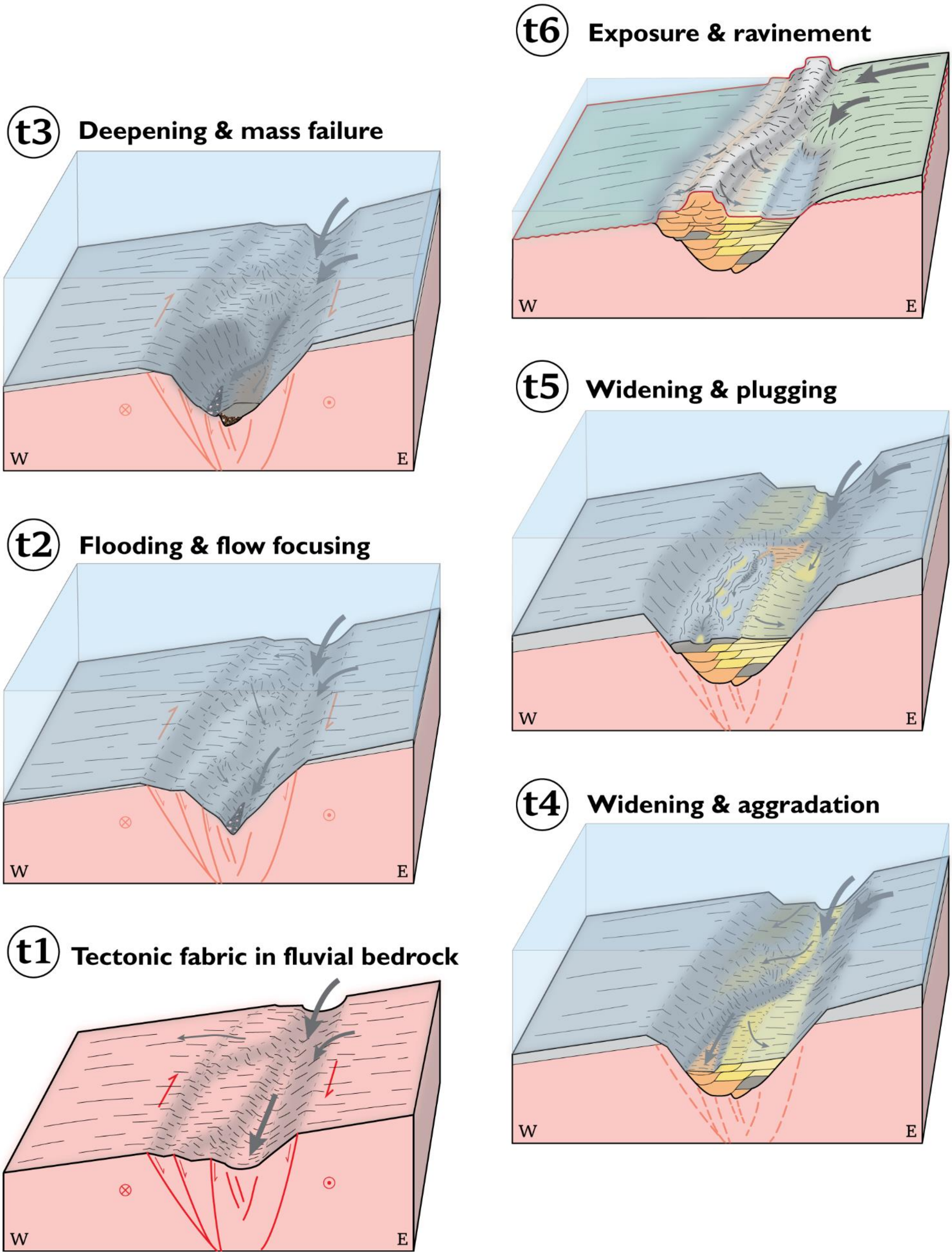

Figure 17: *Evolutionary block diagrams of the Punta Baja canyon as a sediment conduit.* ***t1:*** *Bocana Roja Fm. bedrock: Braided river and floodplain deposits from an eastward source. Releasing-bend tectonics create local depression on regional westward sloping basin margin.* ***t2:*** *Flooding of the basin margin. Submarine gravity flows are captured and focussed by the developing structural depression. Focussed, highly energetic flows erode and entrench the nascent canyon floor.* ***t3:*** *Erosional and tectonic deepening cause lateral and retrogressive canyon wall collapses. Most mass wasting deposits are eroded in the high-gradient erosional canyon thalweg. Canyon widening allows flow expansion, flows become more depositional. Severe thalweg gradient changes caused by mass wasting deposits induce knickpoint development.* ***t4:*** *Canyon widening and backstepping causes deposition and aggradation. Overbank developing in the form of canyon terraces. Thalweg migration through knickpoint migration leaves lateral step channel margin remnants.* ***t5:*** *Further canyon widening through flank collapse plugs thalweg, blocking and/or diverting flows. Canyon floor is wide enough for internal levee development.* ***t6:*** *Relative sea level lowering, ravinement surface erodes an unknown thickness of canyon fill and bedrock. Differential weathering produces more erosion in overbank lithologies, where shallow marine and conglomeratic tallus sediments deposit.*

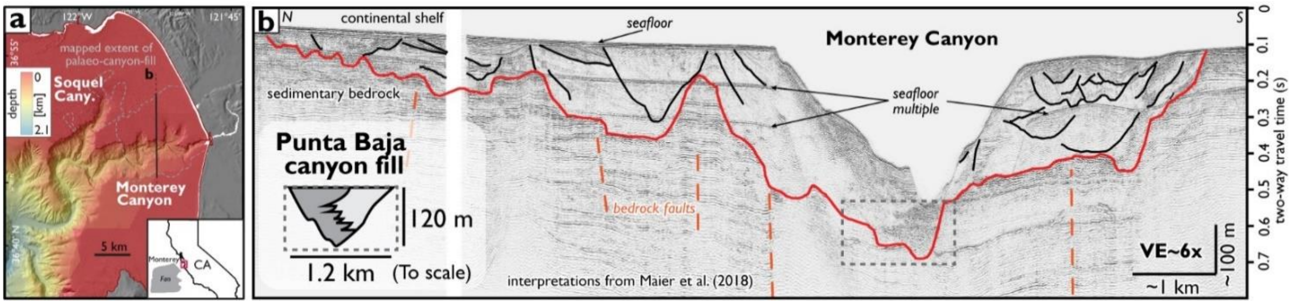

Figure 18: a) *Map and* ***b)*** *seismic reflection profile through the subsurface of Monterey Bay (Map and profile with interpretations modified with permission from Maier et al. (2018)). The red line in b) denotes a composite erosion surface separating the transpressionally deformed Miocene-Pleistocene sedimentary Purisima Formation below from the Pleistocene palaeocanyon sediments above. Black lines are erosional bounding surfaces of palaeocanyon fills. Note schematic inset of the Punta Baja canyon fill dimensions, to scale. The scale and asymmetric internal architecture of the Punta Baja canyon fill is similar to the deepest palaeocanyon incision and fill indicated by the dashed box. Also note that the sedimentary fill is only a fraction of the dimensions of the open canyon conduit. Seismic reflection data available from the U.S. Geological Survey via Balster-Gee et al. (2018).*

Table 1: Facies descriptions

	A	B	C	D	E	F
1	**Code**	**Name**	**Statistics**	**Description**	**Interpretation**	**Fig. 5**
2	Fm	Massive mudstone	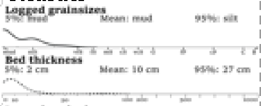	Massive structureless mudstone, commonly rich in sub-mm scale organic material.Deposits from hemipelagic suspension fallout, or low-density turbidity currents that are too fine-grained to differentiate by the naked eye (Boulesteix et al. 2019).	Deposits from hemipelagic suspension fallout, or low-density turbidity currents that are too fine-grained to differentiate by the naked eye (Boulesteix et al. 2019).	a
3	Fl	Laminated mudstone		Laminated mudstone and siltstone, continuous or discontinuous laminae, common mm-scale organic material.	Deposits from hemipelagic suspension fallout, or low-density turbidity currents that are too fine-grained to differentiate by the naked eye (Boulesteix et al. 2019).	b
4	H	Heterolithics		Thin-bedded alternations of mudstone and sandstone, commonly planar laminated to ripple cross-laminated.	Sedimentation by low-density turbidity currents, resulting form the more dilute parts of gravity flows.	c,d
5	ST	Turbidite sandstone	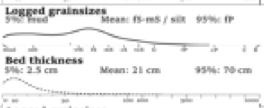	Medium- to thick-bedded sandstones and siltstones, dominantly normally graded, massive or planar laminated to ripple laminated. Common mudclasts and outsized clasts.	Sedimentation by high- and low-density turbidity currents.	e
6	Sl	Low-angle x-laminated sandstone		Medium- to thick-bedded sandstone with low-angle cross-lamination, commonly truncations in multiple directions and diverging/converging laminations.	Deposition from supercritcal turbidity currents (Slootman et al. 2020), variable angle due to reflection off topography. Or shallow-water strandplain aggradation.	f
7	Sw	Wave-rippled sandstone	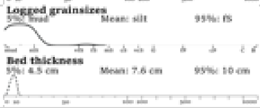	Sand- and siltstone with symmetrical cross-laminations. Sideritic concretions and organic material common.	Sedimentation from oscillatory flow above fair-weather wave-base.	g
8	Dm	Mudclast breccia	(No statistics)	Angular mudclasts in a matrix of sandstone or mudstone. clast-supported or matrix supported. Clasts may be oriented sub-horizontal	Product of the erosion of poorly lithified, but solidified, mud-rich sediments. Transport distance is minimal.	h,i
9	CSh	Horizontally interstratified conglomerate and sandstone	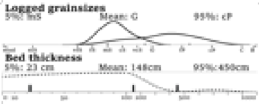	(Sub-)Horizontally stratified conglomerate and sand couplets.	Produced by high-density turbidity currents, multiple pulses either within a single event or within multiple events (Cronin 2018).	j
10	CSx	Cross-stratified conglomerate and sandstone		Dune-scale cross-stratified conglomerate and sand couplets.	Dune gravel barforms, resulting from high-density turbidity currents tractionally reworking or transporting clasts as dunes or sandwaves (Cronin 2018).	j,k,l,m
11	Co	Organised conglomerate	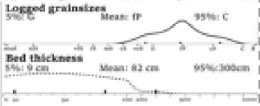	Clast-supported conglomerate with a preferred clast fabric. Normal or reversely graded. Occasionally cross-stratified.	Non-cohesive debris flow (Postma et al. 1988; Lowe 1982; Cronin 2018). Inverse grading when dispersive pressure is high at base of flow, normal grading when dispersive pressure lower (Walker 1975).	n
12	Cu	Unorganised conglomerate	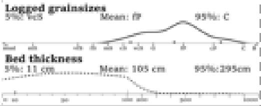	Clast- or matrix-supported poorly-sorted conglomerate with a high poorly-sorted matrix content. Normally , inversely, or non- graded.	Grainflow or en-masse freezing of flow (Walker 1975), related to local failure and short-runout transport of oversteepened deposits with non-cohesive debris-flow characteristics (Nemec 1990; Cronin 2018)	n,o
13	Slump		(No statistics)	Rotated to plastically deformed deposits.	Slope failure with coherent behaviour: short transport distance, immature mass transport deposit.	p
14	Debrite		(No statistics)	Mud-rich intervals with with disintegrated bedding.	Slope failure with complete disaggregration: longer transport distances, mature mass transport deposit.	q